Novel Approach to Protein Crystallizations;

Control of the Phase Behavior of Aqueous Solutions using Microfluidics

A Dissertation

Presented to

The Faculty of the Graduate School of Arts and Sciences

Brandeis University

Department of Physics

Dr. Seth Fraden, Advisor

In Partial Fulfillment

of the Requirement for the Degree

Doctor of Philosophy

by

Jung uk Shim

February 2007

This dissertation, directed and approved by Jung uk Shim's Committee, has been accepted and approved by the Faculty of Brandeis Univeristy in partial fulfillment of the requirement for the degree of;

DOCTOR OF PHILOSOPHY

_____

Gregory Freeze, Dean of Arts and Sciences

Dissertation Committee;

_____

Dr. Seth Fraden,

_____

Dr. Robert B. Meyer, Chair

_____

Dr. Dagma Ringe, Dept. of Biochemistry and Chemistry, Brandeis Univeristy

ACKNOWLEDGEMENTS

He said to them, "How many loaves do you have? Go look!"
And they found out, they said, "Five and two fish". (Mark 6:38)

There are so many people I'd like to thank. First and most especially, I thank Jesus Christ who allows me to lean on him at any moment whenever I need, and enables me to study abroad at this age with my family.

I would really thank my advisor Prof. Seth Fraden who taught and guided me, and spoke with me like a friend. I also thank my lab friends, Kirstin, Josh, Hakim, Phil, Seila, Yanwei, Kate, Jason, Jen, Matt, Greg, Keunho, Zengdong, Darren, David. And, I sincerely thank Samsung who supported me for years.

I thank my wife, Myoung ok, from the bottom of my heart. She taught how to know I have been blessed, and she has been looking at where I am looking at. I thank my mom, dad, parents in law, brothers, sisters, my daughter Suyoun and son Jaeheon.

I pray that I will always be thankful for everything, whatever I do, anywhere I live.

이르시되 너희에게 떡 몇 개나 있느냐 가서 보라 하시니
알아보고 가로되 떡 다섯 개와 물고기 두 마리가 있더이다 하거늘
(마가복음 6:38)

감사를 드리고 싶은 분들이 너무 많아 어디서 부터 감사를 시작해야 할지 알 수 없습니다. 우선 이 나이에 가족과 함께 머나 먼 이곳에 와서 공부하고 생활할 수 있는 기회를 주셨으며 항상 붙잡아 주시고 힘들고 어려울때 의지하게 하신 하나님께 감사를 드립니다.

그리 똘똘하지도, 그리 부지런하지도 않은 이 학생을 때로는 가르치고 훈련시키고, 때로는 친구처럼 삶의 이야기를 나누기도 했던 선생님 Prof. Seth Fraden 에게 감사합니다. 같이 일했고 조언과 도움을 아끼지 않았던 Kirstin, Josh, Hakim, Phil, Seila, Yanwei, Kate, Jason, Jen, Matt, Greg, 근호씨, Zengdong, Darren, David 모두에게 깊은 감사를 드립니다. 또한 이곳에서 살수있도록 현실적인 도움을 주신 삼성전자에 진정으로 감사를 드립니다.

저 먼곳에 서 있던 나를 하나님 옆으로 올 수 있게 하는 계기가 되었으며, 항상 든든하게 내 옆에 서서 내가 바라보는 곳을 같이 바라보는 “마눌님” 명옥이에게 감사합니다. 먼 곳에 계시지만 저와 저희 가족을 위하여 늘 기도하시고 바라시는 아버지, 엄마, 장인어른, 장모님, 동생 재욱이와 진욱이, 형님들, 호준이, 또한 딸네미 수연이, 아들네미 재헌이에게도 감사 드립니다.

이후 어느 곳에서 무슨 일을 하고 살더라도 항상 감사하며 살기를 기도합니다.

ABSTRACT

Novel Approach to Protein Crystallizations;

Control of the Phase Behavior of Aqueous Solutions using Microfluidics

A Dissertation presented to the Faculty of the Graduate School of Arts and Sciences of

Brandeis University, Waltham, Massachusetts

by Jung uk Shim

A microfluidic device denoted the *Phase Chip* has been developed to exploit the permeation of water through poly(dimethylsiloxane) (PDMS) in order to vary the concentration of aqueous nanoliter volume microdrops stored in wells. The permeation of water in the Phase Chip is modeled using the diffusion equation and good agreement between experiment and theory is obtained. The phase diagram of a polymer/salt mixture is measured employing the Phase Chip and agrees well with the phase diagram obtained off-chip. The Phase Chip first creates drops of the polymer/salt mixture whose composition varies sequentially. Subsequently the drops are docked in storage wells and the concentration of each stored drop is controlled by varying the water activity of a reservoir that is separated from the drops by a thin layer of PDMS through which water, but not the solutes, permeates.

The Phase Chip, incorporating a dialysis membrane on-chip, presents several advantages for protein crystallizations. First, protein crystallization is a non-equilibrium process so it makes sense to have dynamic control over the key thermodynamic variable; concentration. The Phase Chip, with its ability to reversibly control protein and precipitant concentrations, renders varying concentration as convenient as varying temperature. Second, by varying the water content of each drop we can explore many different crystallization conditions in the same drop. Finally, we have demonstrated that we can first formulate stable protein solutions, next induce nucleation and then grow large protein crystals. For these reasons, the Phase Chip promises to be a faster, better, and cheaper method for protein crystallization.

This thesis is partially based on the following publications:

1. Jung uk Shim, Galder Cristobal, Darren R. Link, Todd Thorsen, Seth Fraden. Using Microfluidics to Decouple Nucleation and Growth of Protein Crystals. In preparation. – Chapter 4

2. Jung uk Shim, Galder Cristobal, Darren Link, Todd Thorsen, Yanwei Jia, Katie Piatelli, Seth Fraden. Control and measurement of the phase behavior of aqueous solutions using microfluidics. In preparation. – Chapter 3

Contents

List of Tables

List of Figures

Chapter 1

Introduction

1.1 Overview

What is microfluidics? Why is it so interesting scientifically and technologically? The ensuing discussion will attempt to answer those questions, based on several review articles about the subject, such as McDonald et al. (2000)[1], Beebe et al. (2002)[6], Hong et al. (2003)[8], Stone et al. (2004)[9], Squires et al. (2005)[10], Dittrich et al. (2006)[11] and Whitesides (2006)[12], among others.

Microfluidics is the science and technology of systems that control a small amount (10^{-9} to 10^{-18} liters) of liquids in channels with dimensions of between 10 and 100 micrometers. One of its advantages is obviously miniaturizing components and scaling-down processes, therefore leading to reduced-reagent consumption, in addition to expanding a few possible trials into a much larger number of high throughput screenings. Microfluidics has many advantages, particularly its ability to handle and detect small sample volumes, fast system response and processing of biological materials such as DNA, proteins, cells and bacteria.

1.2 Differences caused by Size Reduction

The physical behavior of microfluidic systems deeply relates to their size. One of the most mentioned physical quantities affected by size is the Reynolds number. This is the ratio of inertia to viscous force; $R_e = av/\eta$ with a being the typical dimension of channels, v the speed of flows and η the kinetic viscosity of fluids. The Reynolds number of the micron scale is typically low due to its small dimension. Its range in the microfluidic device is between 10^{-6} to 10. The viscous force, which is the internal friction of a fluid, becomes more significant than inertia that is the tendency of a body in motion to retain its initial motion. Thus, the flow in the systems is linear, or 'laminar'. Laminar flow is smooth and streamlined, unlike the rotating, twisting and unsteady nature of turbulent flows encountered in macroscopic scales where the Reynolds number is high.

Mixing

The lack of turbulence in these systems requires additional mixing processes to blend different fluids and reagents. A few techniques have been developed to enhance the mixing process, such as serpentine channels micro mixer [13, 14], fluid layering [15] and generation of chaotic flow [16, 17]. One of the basic ideas behind mixing technology is the chaotic advection of a flow. A few sets of specially designed grooves on the surface of the channels generate the advection flow that causes the three-dimensional twisting flow in a channel. Changing the extent of the twisting flow by modifying the widths of each groove causes the laminar flow of fluids to become a stream composed of alternate fluid layers. At this small length scale, mixing processes naturally occur by molecular diffusion through the media. For instance, if each of the different fluids in a stream that is

generated by chaotic advection has layers 5 μm thick, it takes 7 ms for salts to diffuse into another layer, since the diffusion coefficient (*D*) of salts is typically $2\times10^3[\mu m^2/\text{sec}]$ with $t = d^2/2D$ where *t* is the time to diffuse and *d* is the distance to travel. The diffusion coefficient of a 5 nm diameter size protein is $40[\mu m^2/\text{sec}]$, so it takes 0.3 seconds to travel 5 μm. The diffusive transport of the protein in the macroscopic scale takes almost 9 days to travel 1 cm distance. Therefore, the diffusion process is more significant in the microscopic scale than in the macroscopic scale.

Drop Formations

A small volume of drops in the continuous phase is an intact platform upon which to accomplish chemical or biochemical reactions, since the drops could confine materials that have been dissolved or suspended within them. One advantage of microfluidics with the spatial confinements feature is that ingredients are mixed faster than processes involving only diffusion. Song et al reported that a set of serpentine channels generates chaotic advections, which accelerates the mixing of fluo-4 and calcium chloride dissolved in drops [14]. The published mixing time of RNase A in Song et al is typically 0.03 seconds. If mixing processes occur only with molecular diffusions, small proteins take about 2 minutes to travel 100 μm, which is the typical diameter of drops, as shown in chapter 1.2.1. In addition, with confinement comes another advantage, which is the ability to manipulate drops without any crosstalk between each of their conditions because of the isolation [9].

The drops can be formed by shearing one liquid into another immiscible liquid [18]. The continuous phase, flowing in a main channel, is inserted by the dispersed phase entering from the perpendicular side channel. The sheer force, exerted by the continuous phase, produces deformation, stretching and eventually rending of the dispersed phase. Therefore, drop formations depend on viscosity and relative velocity, as well as the shape of the microfluidic channels where drops form [19, 20].

The control of drop formation in the microfluidic device could be provided by surfactants and the wetting characteristics of the surface of the channels. A surfactant is an amphiphile composed of a hydrophilic head (water soluble) and a hydrophobic tail (non water soluble). It can lower the interfacial surface tensional force sufficiently, compared to the viscous force, to form drops preferentially [21]. The wetting characteristics of fluids on the surfaces determines which fluid could be drops, and in which continuous phases. A fluid, which is strongly wetter on the surface, should be the continuous phase. The surfactant dependency of wetting property and contact angle is experimentally investigated in Dreyfus et al [22].

Surface to Volume Ratio

The surface to volume ratio is a significant factor in explaining the difference of the physical phenomena shown in microscopic and macroscopic fluid mechanisms. As the dimension reduces, the ratio increases, as does the relative importance of surfaces to volume forces. For instance, if the radius of a sphere reduces from 1 cm to 100 μm, then the surface to volume ratio increases by a 100. So, surface-related forces dominate microscopic phenomena. As mentioned in Stone et al. (2004), a flow of fluids could be

controlled by capillary effect, magnetic field and electric field, which are not significant on the macroscopic scale.

In addition to these external forces, with the chemical and physical properties of the surfaces or geometrical features of the channel, the flows can be controlled in different ways, which are almost impossible to realize in the macroscopic scale. Link et al. showed that the microfluidic channel can break larger drops into precisely controlled smaller drops as a function of the relative resistance of the daughter channels [23]. A microfluidic device can control drop fusions and sorting passively with channel geometries [24], or actively with electric fields [25].

Miniaturized microfluidic devices can offer portability, allowing mobile applications developed for field-disposable systems to detect chemical or biological substances. The ability to perform experiments with very small amounts of precious samples could reduce costs and risks of sample preparations, and make a development cycle faster.

1.3 Applications of Microfluidic Devices

Despite the relatively short history of microfluidic systems, they are considered as one of the most promising experimental or manufacturing tools in various natural and life sciences as well as biotechnology applications.

Currently developed applications include control and detection of biochemical reactions such as DNA analysis by PCR (polymerased chain reaction) [26] or by electrokinetic methods on the PDMS device [27], immunoassay by capillary electrophoresis [28] – for instance, Sia et al reported a portable, low cost microfluidic device to distinguish HIV-1 infected blood from non-infected [29] – cell separations

using an immiscible aqueous two-phase extraction technique [30], and high throughput screening of protein crystallizations [5, 31].

There have been significant attempts to apply microfluidic technology in biology and biochemistry, and there are also many applications realized in the physical sciences such as energy generation using a diffusion-induced fuel cell [32], display technology utilizing electro wettings for reflective displays [33], and environmental technology for detecting leads using a fluorophore labeled cleavage DNA [34].

As iterated in Squires et al (2005) and Whitesides (2006), as microelectronics initiated the integrated circuit revolution, which caused a fundamental alteration to everyday life, microfluidic-based products could also generate a significant impact on human society with precise manipulation of fluids on the microscopic scale while discovering and exploiting new phenomena. Evidently, this requires a great deal of research and effort.

1.4 Protein Crystallizations

Determining the three-dimensional structure of proteins and protein-ligand complexes are key objectives of structural biology and rational drug design, respectively. Central to both fields is the use of x-ray diffraction from protein crystals to deduce structure. The creation of protein crystals from a solution is a difficult problem and the vast majority of proteins have eluded crystallization. Currently there are no established methods through which a measured physical property of the protein can be used to predict crystallization conditions, although there is some indication that solution thermodynamics can provide guidance [35-37]. Typically crystallization trials proceed by trial and error and a new protein is screened against hundreds to thousands of crystallization conditions that have

succeeded in the past using sample volumes to the order of 100 nl [38-41]. It is often difficult to produce the protein in sufficient quantities for all the screenings, hence the motivation to further reduce sample size. This is one of the reasons that the microfluidic system is necessary for protein crystallizations.

1.4.1 What is the Decoupling Nucleation and Crystal growth?

At low protein concentrations, a protein solution is thermodynamically stable. An increase in concentration of a precipitant, such as salt or polyethylene glycol (PEG), drives the protein into a region of the phase diagram where the solution is metastable and protein crystals are stable. In this region there is a free energy barrier to nucleating protein crystals and the nucleation rate can be extremely low. However, once crystals do nucleate, crystal growth is slow because of the shallow supersaturation, which produces defect-free crystals.

At higher concentrations the nucleation barrier is suppressed and nucleation rapidly occurs. Unfortunately, at deep supersaturation, the crystal growth is rapid and defects do not have time to anneal out of the crystal, leading to poor quality crystals. Thus production of protein crystals requires two conditions that work against each other. On one hand to nucleate crystals, high supersaturation is needed, but on the other hand low supersaturation is necessary in order that crystal growth proceeds slowly enough for defects to anneal away.

The solution to this problem is to change sample conditions during the crystallization process. Ideal crystal growing conditions occur when the sample is temporarily brought into the region of deep supersaturation where the nucleation rate is high enough to be

tolerable. In the ideal scenario, after a few crystals have nucleated, the supersaturation of the solution would be decreased by lowering the protein or salt concentrations, or raising the temperature in order to suppress further crystal nucleation and to establish conditions where slow, defect-free crystal growth occurs. In other words, independent control of nucleation and growth is desired.

1.4.2 Non Microfluidic Traditional Methods

In the traditional *vapor diffusion* method, two open containers, one with a microliter of a protein solution and the other with a milliliter of a salt solution, are placed together in a sealed vessel such that the solutions are in contact only through the vapor phase. If the salts, proteins, and polymers are non-volatile, then only water is exchanged between the protein solution and reservoir until equilibrium is reached, at which point the chemical potentials of the water in the protein solution, reservoir, and vapor are equal. For example, if the protein-free reservoir is saltier than the protein solution, then water will leave the protein solution until its chemical potential is the same as in the reservoir. As water leaves the protein solution all the components are concentrated and the protein solution follows the trajectory of the black arrow in Figure 1.1b. Depending on initial conditions, the protein solution can be either concentrated or diluted (the direction of the arrow can be reversed). Vapor diffusion has the advantage that a protein solution can start in a part of the phase diagram where nucleation is high and then move into a region where growth is slow as the vapor diffusion process proceeds. So, vapor diffusion is irreversible.

Microdialysis [39, 42, 43] and crystal seeding [40] have been two methods employed in protein crystallizations that permit independent optimization of nucleation and crystal growth. In microdialysis, several microliters of protein solution are sealed in a container by a semi-permeable membrane and subsequently submerged in a reservoir of fixed chemical potential. Microdialysis allows the changing of solvent conditions so that nucleation and growth can be independently optimized. In the crystal seeding method, solution conditions are first deeply supersaturated in order to nucleate many small crystals, or "seeds". Then a few seeds are transferred to a solution of shallow supersaturation that is optimized for growth. This decoupling of steps allows independent optimization of nucleation and growth. However, crystal seeding as currently practiced is a laborious practice that is not conducive to automation or high throughput.

1.4.3 Microfluidic Implementations

Recently three microfluidic implementations of protein crystallization techniques have been reported. The first, known as *free interface diffusion*, developed by Quake's laboratory [5, 44] has been commercialized by Fluidigm (http://www.fluidigm.com) illustrated in Figure 1.1b. The second microfluidic approach to protein crystallization, developed by Ismagilov [20, 31, 45, 46], is known as *microbatch* and is illustrated in Figure 1.2a. The third microfluidic method is the implementation of vapor diffusion reported by Ismagilov's group [4] illustrated in Figure 1.2b.

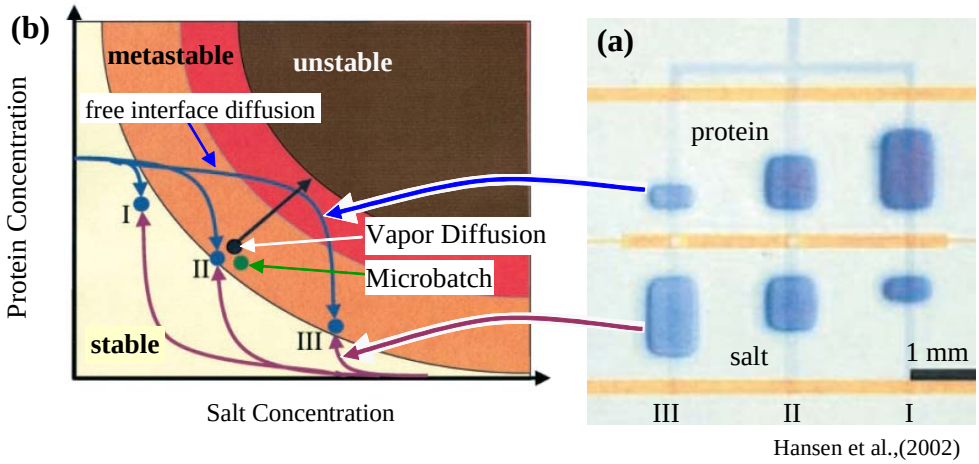

Figure 1.1 (a) Free Interface Diffusion. In the Fluidigm device the protein solution is loaded into the top three cells while a precipitant is loaded into the bottom three cells. The valves (orange lines) between the salt and protein solutions are closed during filling. After opening the valves, salt rapidly diffuses into the protein side, while the protein diffuses into the salt side at a slower rate. **(b)** Generic phase diagram for protein crystallization [5, 7] illustrate free interface diffusion, vapor diffusion, and microbatch. The average concentrations inside the upper (lower) wells numbered I - III in (a) evolve along the upper (lower) of the curves I - III in (b). The blue dots indicate average equilibrium concentrations. For instance, the average composition of upper well III in (a) follows the upper (blue) curve III in (b). Initially, the protein solution is stable, then as salt rapidly diffuses into the upper well the solution moves deep into the metastable region where the nucleation rate is high, and as protein slowly diffuses out of the well the solution finally reaches the equilibrium composition where crystal growth is slow. The vapor diffusion process follows the black arrow while with microbatch (the green dot) the average solution composition is fixed.

Free Interface Diffusion Method

The free interface diffusion approach adopted onto microfluidic devices is to mix a rapidly diffusing salt with a slowly diffusing protein, which can result in producing

solvent conditions that temporarily have a period of high nucleation rate, followed by conditions that lead to slow crystal growth. The trajectory followed by curve III in Figure 1.1b represents this ideal case.

The drawback of free interface diffusion is that the kinetics of traversing the pathways through the phase diagram is both uncontrolled and irreversible. Salt and protein have large differences in diffusion coefficients, as shown in Chapter 1.2.1, which may permit trajectories such as curves I - III illustrated in Figure 1.1, but there is limited control over the duration of residence in the supersaturated region. Furthermore, polymers such as PEG have diffusion constants that are similar to the proteins, in which case the pathway through the phase diagram is a straight line connecting the initial concentrations of two solutions. However, even with these constraints the microfluidic free interface diffusion approach has been successful at finding new crystallization conditions.[44]

Microbatch Method

The second microfluidic approach to protein crystallization, developed by Ismagilov [20, 31, 45, 46], is known as *microbatch* and is illustrated in Figure 1.2a. Here aqueous solutions containing protein, salt, PEG, and buffer are introduced as separate flows and combined into a single stream in the microfluidic device. The solutions are driven into the device with syringe pumps whose flow rate is programmed to vary linearly in time with one component increasing while a second one decreases, but maintaining a constant overall flow rate.

For example, a 2 M salt solution varies from 10 μl/hr to 90 μl/hr, while the buffer varies from 90 μl/hr to 10 μl/hr and the protein solution remains constant at 100 μl/hr. In

this way the protein concentration remains constant, but the salt concentration varies continuously from 0.1 M to 0.9 M. The aqueous stream then encounters an immiscible oil stream and aqueous drops immersed in the oil stream are formed. In a typical device, drops have a volume of 0.1 nl to 1.0 nl and the flow rates are about 100 μl/hr. Under these conditions drops are produced at a frequency of 100 drops/sec. Each drop has a different composition of aqueous reagents, so a combinatorial library of all possible concentrations of the reagents can be produced rapidly.

The path in the phase diagram for Ismagilov's microbatch technique is represented by the green dot in Figure 1.1b. The disadvantage of microbatch is that the protein concentration is fixed. In order for crystals to grow, favorable conditions for both nucleation and growth have to be simultaneously present.

Vapor Diffusion

The third microfluidic method is the implementation of vapor diffusion reported by Ismagilov's group [4] illustrated in Figure 1.2b. They created emulsions of aqueous drops inside a continuous oil phase as with the microbatch method shown in Figure 1.2a. Water is slightly soluble in some oils, such as poly(dimethylsiloxane) [4, 47], while salt and protein are insoluble in these oils. Using a water soluble oil as the continuous phase, a sequence of high concentration salt, protein-free drops alternating with low salt concentration drops containing protein is created. Water diffuses through the oil until the chemical potential of water between drops are equal, which leads to an increase in the protein and salt concentrations in the protein containing drops, driving crystallization. The equilibration time is of the order of several days, which is similar to non-

microfluidic vapor diffusion. Again, like traditional vapor diffusion, Ismagilov's microfluidic implementation is irreversible [4].

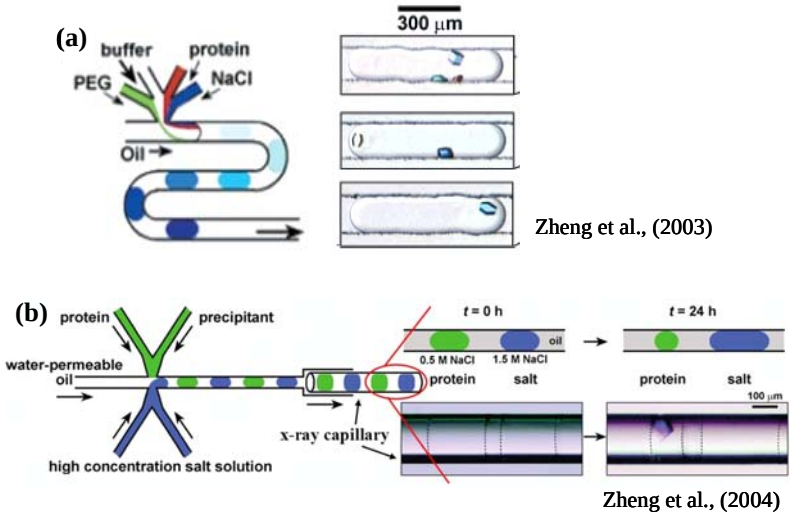

Figure 1.2 (a) Microbatch. Flows of aqueous components are co-joined and then drops are formed when merged with a stream of immiscible oil. Varying proportions of the aqueous components result in drops of different concentrations of reagents. Protein crystals grow in nanoliter-sized drops that are high in salt. **(b) Vapor Diffusion.** Microfluidic implémentations of vapor diffusion [4]. Here the water is slightly soluble in the oil, but salt and protein are insoluble. High concentration salt drops (dark blue) alternate with low salt concentration drops containing protein (light green). Water diffuses through the oil until the salt concentrations are approximately equal, which leads to an increase in the protein and salt concentrations in the green drop, driving crystallization.

1.5 An Outline of this thesis

The goal of this thesis is, firstly, to report developments of a high-throughput low volume microfluidic device, the *Phase Chip*, designed to decouple the physical processes of protein crystal nucleation and growth by exploiting the reversible controllability of

chemical potentials of water through PDMS membrane. We have demonstrated that by cycling the protein concentration we can first formulate stable protein solutions, next induce nucleation and then grow large protein crystals.

The second goal is to understand the water permeation in the Phase Chip while controlling the concentrations of reagents dissolved in stored drops. The permeation of water is modeled using the diffusion theory and good agreements between experiment and theory are obtained. In order to ascertain the usefulness of the Phase Chip for the control and measurement of the phase behavior of aqueous solutions, the phase diagrams of PEG/ammonium sulfate solution were measured on-chip and off-chip.

Chapter 2 explains the development of a microfluidic device, made out of PDMS, which can store drops in specific docking sites and reversibly and controllably vary the concentration of solutes in the drops.

Chapter 3 describes that the permeation of water in the Phase Chip can be modeled using the diffusion equation, and the phase diagram of a polymer/salt mixture can be measured employing the Phase Chip and agrees well with the phase diagram obtained off-chip.

Chapter 4 shows that proteins can be crystallized and melt with respect to the reservoir condition, and the Phase Chip can drive the protein solution into the deep supersaturation, after nucleation happens, take them back into shallow supersaturation to enhance the crystal growths while lowers the nucleation rates.

Chapter 2

Device Developments

Microfluidic instruments are capable of precisely manipulating sub-nanoliter quantities of fluids. Their purpose is to vastly reduce the amount of fluids used in chemical processing and provide accurate delivery of fluids in a defined geometry on the micron length scale with a temporal accuracy of milliseconds.

A microfluidic device can include channels for transporting fluids, valves for controlling flow, nozzles to create drops, pumps to propel fluids, storage chambers for drops and streams, and mixers to homogenize multiple fluid streams and drops [48]. The individual primitive functions could be properly combined in numerous ways to perform the biological or chemical manipulation on the fluid of nanoliter volume. In addition to the synergic systems, we add the ability to controllably vary the water contents of the drops.

This chapter describes the development of a microfluidic device, the Phase Chip as shown in Figure 2.1, which can store drops in specific docking sites and reversibly and controllably vary the concentration of solutes in the drops.

2.1 Overview

The Phase Chip is a poly(dimethylsiloxane) (PDMS) device, which utilizes hydrodynamic focusing to produce drops of aqueous solution inside a continuous oil stream [10, 31, 49].

Figure 2.1 shows a global view of the Phase Chip. It has four injection holes to insert tubings for introducing fluids into the device; the outer two for oil and the inner two for the aqueous solution. The winding channel, the mixer, generates chaotic advection, which folds and stretches the drop when passing the corners [46, 50]. The mixer blends the multiple solutes of drops.

There are four storage regions in which the device can store the drops that are carried through the flow channel (refer to Chapter 2.4), which is made out of negative photoresist (refer to Chapter 2.3). Each storage region has an entrance and an exit valve to control the stream of drops that flow into the area.

One valve consists of a valve layer, which is a flow channel made out of positive photoresist, and the control channel that is placed underneath to deflect the valve membrane to seal off the valve layer (refer to Chapter 2.6). When these valves are open to guide the stream into the storage region, the main valve have to be closed, otherwise almost all of the drops will flow out through the waste exhaust because of the lowest flow resistance that is linearly proportional to the length of the channel [6].

Once the storage region contains drops that have solutions of combinatorially varied compositions [31], in order to concentrate or dilute solutes dissolved in solutions that are stored in wells, the chemical potential of water is applied by introducing the high salt solution or water into the reservoir (refer to Chapter 3.2).

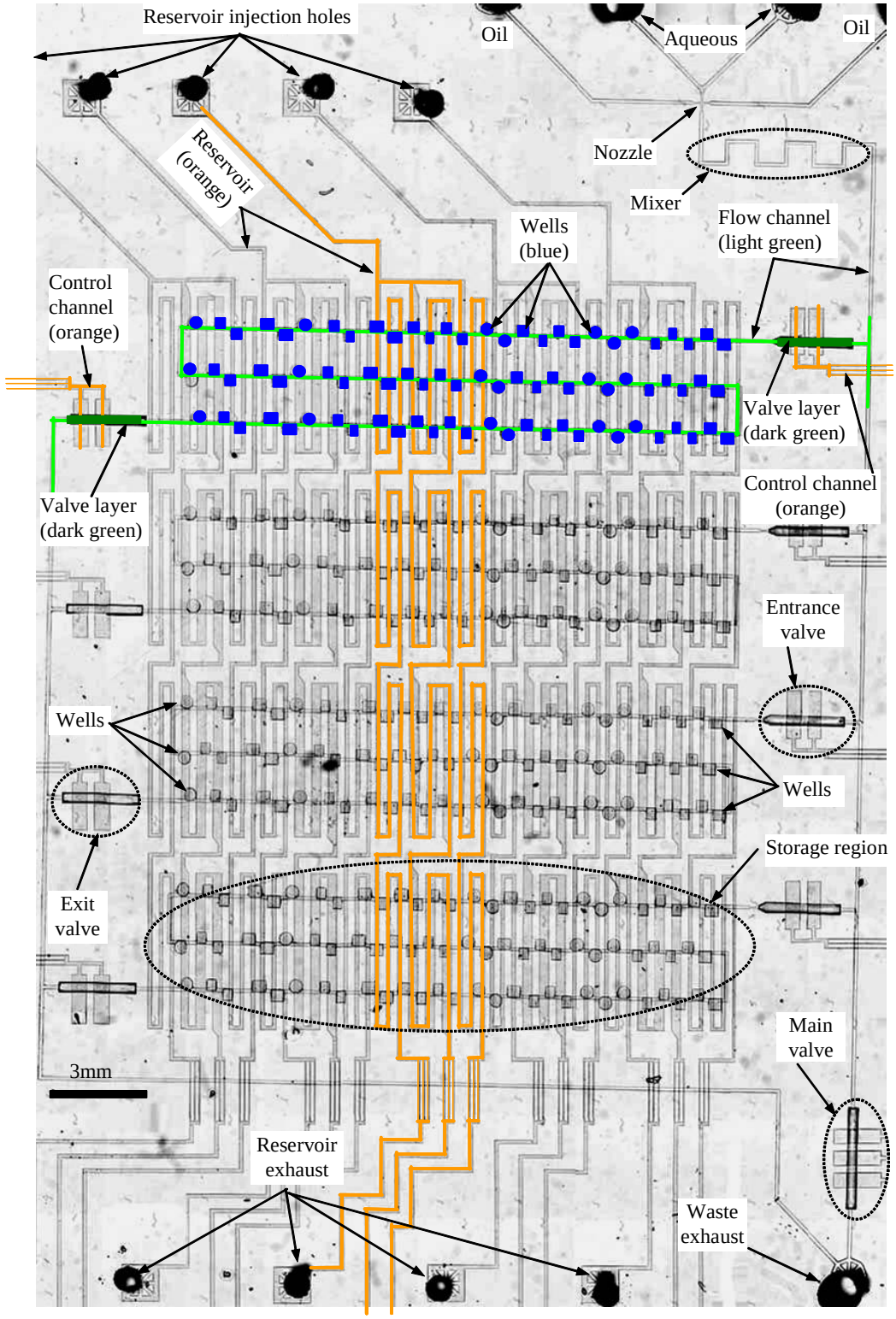

Figure 2.1 The global view of the Phase Chip. It is a stitched photograph.

The reservoir consists of five independent serpentine channels, so five different chemical potentials can be applied to the storage regions. A device has 4 storage regions, and each region has 84 wells with 5 different reservoir conditions, so the maximum possible number of screenings for each device is 1680. And, if it is feasible to inspect each well while the drops are shrinking or swelling, the number of screening are enormous.

While the water exchange occurs through the dialysis membrane, the storage area needs to be isolated by the closure of all injection holes and the waste exhaust. However, PDMS absorbs water, organic solvents and even some fluorinated fluids from the storage area [51, 52] (refer to Chapter 2.8), so it is necessary to supply the oil to the device while controlling the concentrations of drops for maintaining the system's stability. In order to continue supplying oil during the dialysis process, a tubing connected to the waste exhaust conveys oil under constant pressure while all other injection holes are sealed with plugs. Because the oil is forced to flow into channels under constant pressure, there is virtually no oil flow, which allows the experiment to take place uninterrupted in the wells while it prevents the storage area from drying out of oil.

2.2 Mask Design

Figure 2.2a shows the mask design plotted with AutoCAD (Autodesk Inc.,), which is comprised of four different layers; the flow channel (light green), the valve layer (dark green), the well channel (blue) and the reservoir/control channel (orange). When drawing the mask, I have a few of my own requirements.

The shortest distance between patterns on the same layer is 200 μm. The safety distance prevents bridge defect, in which two patterns are connected by process errors from being too close together or encountering a particle sitting on the spot.

Patterns representing any functional tool of the device shouldn't be placed within 14000 μm from the edge of the wafer. If a pattern is too close to the edge, the edge is usually abnormally thick because of the edge bidding effect. That is caused by the surface tensional retraction of the photoresist while they are still viscous liquids after spinning. And, the location of a pattern on a wafer is also restricted by the size of the glass substrate that is used as a counter face of the channel when fabricating the PDMS device.

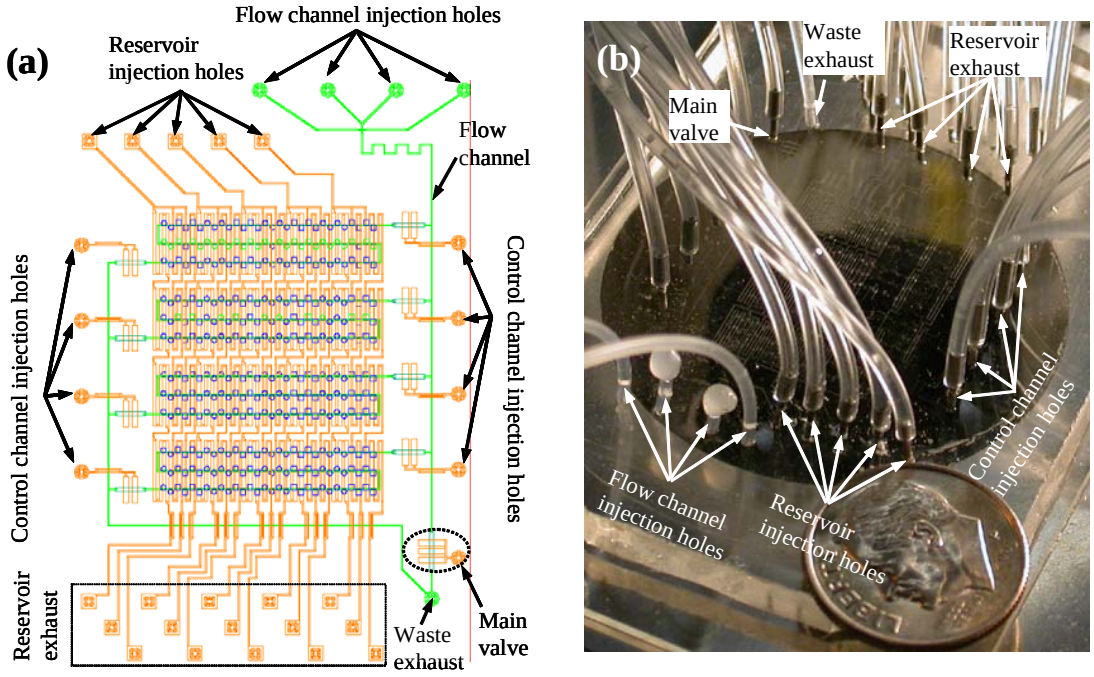

Figure 2.2. (a) A microfluidic design drawn using AutoCAD. The drawing will be transferred on the transparency film (a mask). **(b)** The photograph shows the actually running Phase Chip. It shows the device preparation step, which fills the flow channel with oil. Aqueous solutions will be injected through the two inner injection holes, closed by two plugs as shown in the left-lower side of the photograph.

If two different patterns are connected on the same layer - for example the valve layer and the flow channel, which are made out of positive and negative photoresist respectively - there has to be an overlap of 100 μm between them. They are carved with two separate photolithography, so it is necessary to align the second mask on the wafer with inscribed the first patterns to properly connect the two different patterns. The overlap compensates for the misalignment of the mask on the wafer and the fluctuation of the develop process. However, if the two patterns are connected on different layers - for example the flow channel and the well layer - the 10μm margin is enough to compensate for process errors.

There is another misalignment margin in the design. It comes from the placement of the thick PDMS slab onto thin PDMS layer, which is spun on a wafer. Because the alignment is performed manually, holding a thick PDMS slab and placing it on a wafer, the error depends on personal experiences. I give a margin of 850 μm on the design.

Figure 2.2b shows the Phase Chip running. The tubings connect the microscopic device with the macroscopic outside world. We use Polyethylene tubing for the injection of solutions, and employ TYGON tubing for introducing pressure to actuate valves and for circulating fluids into reservoirs to build the chemical potential.

2.3 Device Fabrication

The early version of the microfluidic devices were manufactured on silicone wafers and glass to take advantage of the technology already developed in microelectronics and MEMs (Micro Electro Mechanical systems)[53, 54]. However, the fabrication of the device made out of glass and wafer requires rather troublesome processes, like annealing

the device at high temperatures to close the channel with a glass cover on wafer, drilling the holes through the glass into the reservoir, which is a time and labor intensive process [55].

Even though the microfluidics based on the micromachining is very attractive, the polymer microfluidics has a lot more advantages than the earlier version. We have been developing the microfluidic devices composed of PDMS (poly (dimethylsiloxane)). PDMS is excellent material to manufacture microfluidic systems for a number of reasons. Microscopic features on a wafer can be easily sculptured on PDMA with high reproducibility by replica molding. And, the process conditions are accessible - for instance low curing temperature, non-toxic properties of PDMS and sealing compatibility with many substrates [1]. PDMS is less expensive than wafers, and engages in the less complicated processes to be constructed. Also, it is usually transparent so that it is possible to optically detect the reaction in the device, such as UV/Visible light absorbance and fluorescence [56-58].

2.3.1 Photolithography

As shown in Figure 2.3a, the first step in converting a microfluidic design concept into a laboratory instrument consists of drawing the microfluidic circuit. The drawings are produced using a computer aided design program, AutoCad (AutoDesk Inc.) as shown in Figure 2.2a. High resolution photo masks are fabricated rapidly on transparencies by a specialized company (CAD/Art Services Inc., OR). Each transparency can accommodate six different masks designed for three-inch silicon wafers.

Next, a silicon wafer (3inches silicon wafer, Silicon Sense Inc.,) cleaned with solvents is spin-coated with the photoresist (SU8-2025, Microchem Inc., AZ-P4903, Clariant Inc.,) with typical thicknesses ranging of 7 ~ 50 μm.

SU8-2025 is the negative photoresist, in which the portion of the photoresist that is exposed to UV light becomes relatively insoluble to the developer (1-Methoxy-2-Propanol Acetate, Sigma-aldrich). The unexposed portion of the photoresist is dissolved into the developer. It is a high contrast, epoxy-based photoresist designed for micromachining and microelectronic application, where a thick, chemical and thermal stability is required [59]. The photoresist is most commonly reactive with the near UV (350 nm ~ 400 nm) light, although i-line (365 nm) is preferable. When exposed to UV light, the crosslinking process happens in two steps; formation of a strong acid activated with the exposure process followed by acid-initiated, thermally driven epoxy crosslinking during the post exposure bake (http://www.microchem.com). Negative photoresist is used to fabricate the flow channel, well layer and reservoir/control channel.

AZ-P4903 is the positive photoresist, in which the portion of the photoresist that is exposed to UV light becomes soluble into the developer and the portion of the photoresist that is unexposed remains insoluble. The positive photoresist is a thermoplastic polymer that becomes soft on heating above the glass transition temperature and melt, it can be molded again after develop process. Repetitive heating of thermoplastics does not cause permanent change in properties or composition. Positive photoresist is employed to build the valve layer that shows better performance if its cross section is rounded shape [3].

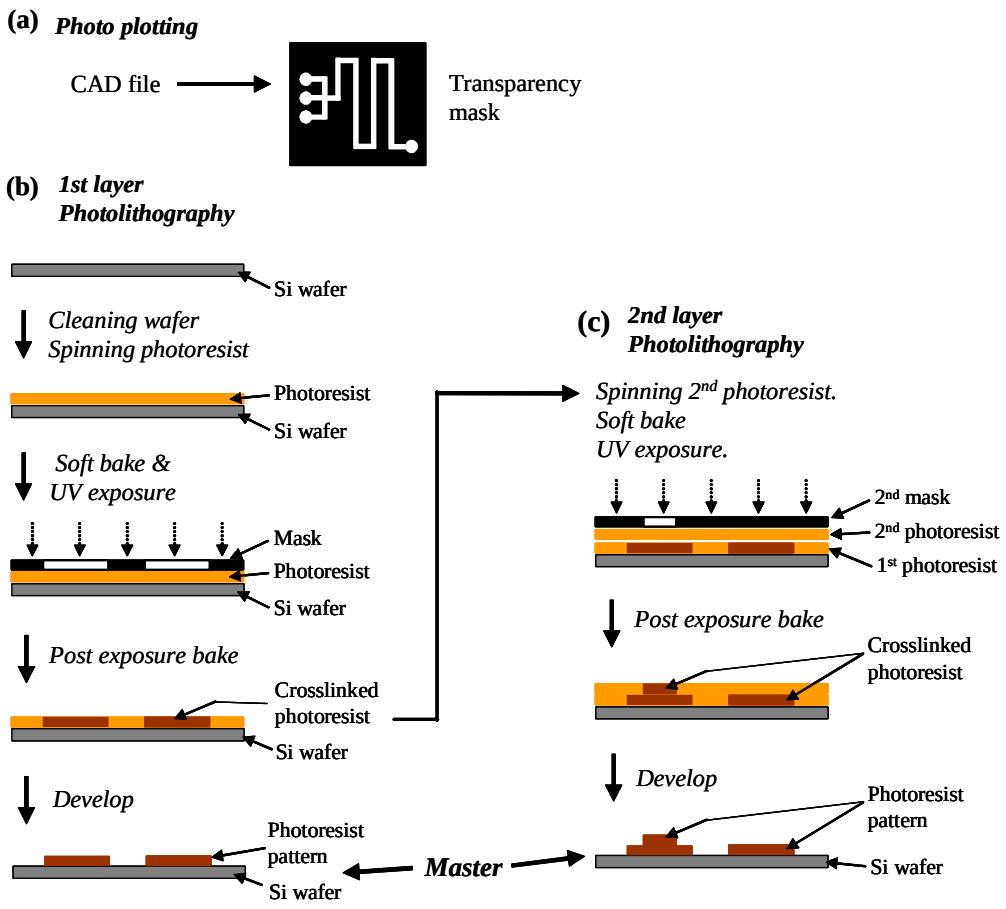

Figure 2.3 Photolithography processes for a negative photoresist. **(a)** A microfluidic design is drawn using a CAD program and a photomask is photoplotted on a transparency. **(b)** Photoresist is spun on a silicon wafer. The resist is exposed to UV light through a mask and baked, which crosslinks the resist. Unexposed resist is developed away. **(c)** To manufacture 3D structure, an additional photoresist is photolithographed.

As illustrated in Figure 2.3b, a mask is placed in contact with the wafer and UV light exposes on the photoresist through the mask. Figure 2.3 demonstrates the photolithography process for negative photoresist. When a coated, exposed wafer is placed in the developer, the unexposed photoresist dissolves, leaving the patterns that are exposed, crosslinked photoresists, attached to the silicon wafer (Figure 2.3b). This wafer

having sculpted patterns is referred to as the “master”. In order to make 3-dimensional structures such as the well layer on the flow channel, an additional photolithography, involving the second spin coating of the negative photoresist, aligning the mask onto the master and the second UV exposure, is necessary as illustrated in Figure 2.3c.

2.3.2 Softlithography

The procedure of construction of microfluidic devices in PDMS, known as “soft lithography,” is illustrated in Figure 2.4 and has been reviewed in the literature [48].

A commercially available liquid PDMS kit comes with a pre-polymer and a crosslinker (Sylgard184, Dow Corning). The mixed, degassed liquid PDMS is poured onto the master and then cured by baking at 65 ˚C for 25 minutes. The resulting transparent, flexible silicone rubber is peeled off the master, leaving relief features from the master imprinted onto the PDMS slab. Injection holes are punched through the PDMS in order to insert tubing that will carry the fluids that are introduced into the device.

At this point the PDMS slab has channels that are open on one surface and need to be sealed. The PDMS is directly bonded to glass by exposing both surfaces to an oxygen plasma and then placing the two surfaces in contact as in Figure 2.4a. Since the oxygen plasma discharge transforms –OSi(CH3)2O– groups on the surface of the PDMS into –OnSi(OH)4-n, the siloxane covalent bond –Si–O–Si– bridged by the condensation reaction between the surface of PDMS and glass creates a strong, irreversible seal [60].

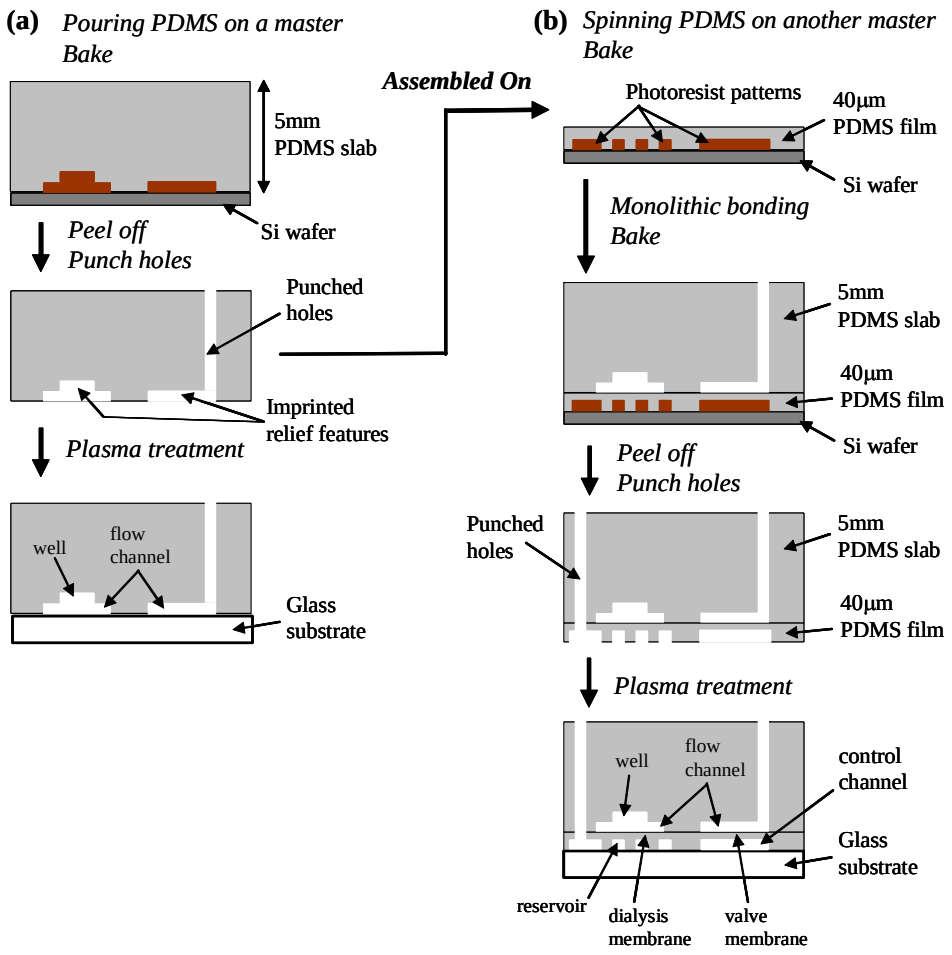

Figure 2.4 Microfluidic device fabrication using soft lithography. **(a)** Liquid PDMS is poured onto the master and then cured at 65 ˚C. The soft elastomer is peeled off, leaving patterns embossed in the PDMS. Access holes are punched through the PDMS which is then bonded to a glass substrate by an oxygen plasma treatment, **(b)** or to another PDMS layer containing the control channel and the reservoir (multi layer soft lithography).

In order to fabricate the control channel and reservoir in the Phase Chip, a thin PDMS layer should be added on the face of the PDMS slab before closing the face with a glass substrate. The Phase Chip, which is a multi-layered device, is made out of two masters. One master has the flow channel, the valve channel and the well layer. The other master has the control channel and reservoir. The ratio of 10:1 in weight is the recommended

proportion of pre-polymer and crosslinker respectively, however, when making the multi-layer device, the weight ratio for the thick PDMS slab is 5:1, and 20:1 for the thin PDMS layer. Each layer has an excess of one, a deficiency of the other. The thick PDMS slab (~5mm) is cast from a master having the flow channel on it by pouring the 5:1 ratio liquid PDMS. As illustrated in Figure 2.4b, the thin PDMS layer (~40 μm) is formed by spinning 20:1 ratio of liquid PDMS on another master having control channel, and cured at 85 ˚C for 5 minutes.

Each PDMS layers are cured partially as long as the surfaces are tacky. We speculate that there are some uncured crosslinkers left in the thick layer as the latter had an excess of crosslinkers. After the curing, the thick layer is removed from one master and placed onto the other master already having the thin PDMS film spun on it. When placing one onto the other, a precise optical alignment is required to put the valve channel above the control channel, and the reservoir underneath the well.

After that, they are baked again at 85 ˚C for 30 minutes to enhance the bonding between them. While baking, the excess of crosslinkers diffuses from the thick layer into the thin layer where they are deficient [61]. Further curing causes the two layers to form crosslinked elastomer at the interface. This process makes a monolithic multilayer PDMS device that has the flow channel and the well on the upper layer, and the control channel and reservoir on the bottom layer.

The two-layer PDMS slab is peeled off the master. The injection holes are punched with the lure stub adapters in order to insert tubings, and it is cleaned by the dry nitrogen gas. The slab has the control channel and the reservoir that are open on one surface. In order to close the open face, the slab and a glass substrate are exposed to a oxygen plasma, placed one on another to form a very tight, irreversible seal [60]. The detail of

the process condition for fabricating the master and the PDMS molding are described in Table 2.1.

(a)

Pre treatment			-. Rising a wafer with methanol, Isopropyl alcohol (IPA) -. Air blowing
Flow channel	1st PR* coating	-. PR: SU8-2025 thickness: 30μm	-. Spinning: 0rpm → 800rpm / 5sec → 2800rpm / 60sec 100rpm/s 300rpm/s : ramping -. Soft bake: 65˚C / 2min → 95˚C / 5min
	1st Exposure	-. Mask Id: Flow	-. Exposure time: 15sec -. Post exposure bake: 65˚C / 2min → 95˚C / 4min
Well Layer	2nd PR coating	-. PR: SU8-2007 thickness: 7μm	-. Spinning: 0rpm → 800rpm / 5sec → 2800rpm / 60sec 100rpm/s 300rpm/s : ramping -. Soft bake: 65˚C / 1min → 95˚C / 2min
	2nd Exposure	-. Mask Id: Well	-. Exposure time: 10sec -. Post exposure bake: 65˚C / 1min → 95˚C / 2min
	Develop		-. Developer: 1-Methoxy-2-Propanol Acetate -. Rinsing with IPA
Valve Layer	3rd Coating	-.PR: AZ-P4903 thickness: 40μm	-. HMDS# treatment. -. Spinning: 0rpm → 500rpm / 3sec → 1500rpm / 60sec → 500rpm / 0sec (raping rate: 100rpm/sec) -. Wait 10min -. Soft bake: 65˚C / 3min → 105˚C / 5min
	3rd Exposure	-.Mask Id: Valve	-. Exposure time: 50sec
	Develop		-. AZ400k% diluted 4 times with DI water -. Rinsing with water
	Reflow		-. Bake: 70˚C → 110˚C / 10min (ramping)
Control channel	PR coating on another Wafer	-. PR: SU8-2025 thickness: 30μm	-. Spinning: 0rpm → 800rpm / 5sec → 2800rpm / 60sec 100rpm/s 300rpm/s : ramping -. Soft bake: 65˚C / 2min → 95˚C / 5min
	1st Exposure	-. Mask Id: Control	-. Exposure time: 15sec -. Post exposure bake: 65˚C / 2min → 95˚C / 4min

PR*: Photoresist, HMDS#: hexamethyldisilazane, AZ400k%: the developer for AZ-P4903, Potassium Borates

(b)

Thick PDMS slab	-. Pouring 5:1 ratio PDMS on a master contained in a Petri dish. -. Baking at 65˚C for 25min in a oven. -. Peeling off and Punching Holes.
Thin PDMS film	-. Spinning 20:1 ratio PDMS on the other master. recipe: 0rpm → 800rpm / 5sec → 2000rpm / 60sec -. Baking at 85˚C for 5min on Hot plate.
Assembling	-. Aligning and Placing thick slab on thin film PDMS. -. Annealing them at 85˚C for 30min on Hot plate. -. Peeling off and Punching Holes. -. Bonding it on a glass substrate with the oxygen plasma treatment

Table 2.1 (a) The detail conditions of Photolithography, **(b)** of multilayer Soft Lithography.

2.4 Isolation of Drops

One of the significant advantages of the microfluidic system is its ability to reduce the reactor size [62]. As shown in Figure 2.5a, the protein solution is loaded into the top three cells while a precipitant is loaded into the bottom three cells and the valves (orange lines) between the salt and protein solutions are closed during filling [5]. This setup is for the protein crystallization method known as the Free interface diffusion method. The chamber and the valves prevent interruptions from happening in the solution. Ismagilov's group presented a microfluidic implementation of vapor diffusion [4], illustrated in Figure 2.5b. They created alternating compositions of the aqueous drops inside continuous oil phase, and allowed them to flow into a glass capillary to isolate the drops. The water is exchanged through the oil until the chemical potential of drops is equilibrated. In order to modify or control the concentration of solutes dissolved in the solution, the solution should be placed in the defined place in the microfluidic device.

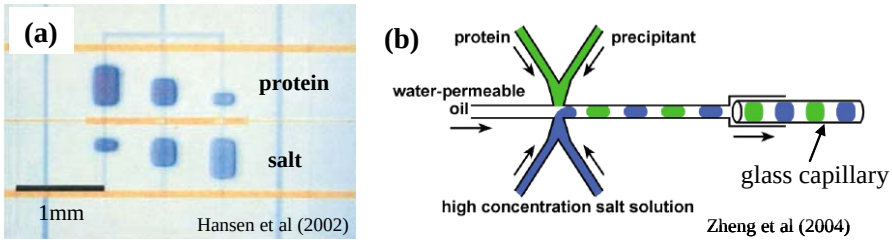

Figure 2.5. In order to evaluate chemical and physical reactions in the micron size, the solutions should be insolated from the environment. **(a)** The protein solution is loaded in the upper cells, and the salt is loaded in lower cells. The height of cells is same as the flow channel. After the valve in the middle (orange) open, the two kinds of solutes diffuse to each other [5]. **(b)** The alternating drops of solutions of salt and protein formed at the nozzle are loaded into the glass capillary. The capillary is removed from the PDMS device and inspected [4].

2.4.1 Why does a Well attract Drops ?

Isolating drops in the Phase Chip is carried out with an achievement of the surface tension forces to guide each drop to a storage well, illustrated in Figure 2.6. After the drops are formed, they are forced to flow through channels of wide width (100 μm), but narrow height (30 μm), which flattens the drops and creates a large surface area, and because of the oil-water interface, a large surface energy. Wells are fabricated on the device that are adjacent to but still connected with the flow channel. Because the wells are deeper than the channel, a drop inside the well will assume a more spherical shape, which lowers the surface area of the drop. The gradient in the height of the microfluidic device produces a gradient in the drop's surface area, therefore a gradient in the interfacial energy that generates a force on the drop, driving it out of the confining channel into the deeper well.

For example, the shape of a drop is assumed to be an elongated rectangle when it is flowing in the flow channel, and the shape is assumed to be a sphere when stored in a well, as shown in Figure 2.6. After the drop is docked into the well, the area is smaller, and the center of mass is higher than when the drop flows in the channel. So, there is a gravitational energy gain and a surface tensional energy loss when the drop moves from the flow channel to the well. The surface tensional energy loss is approximately 10000 times higher with typical parameters, therefore, the drops are preferentially docked into the wells rather than flowing through the channel.

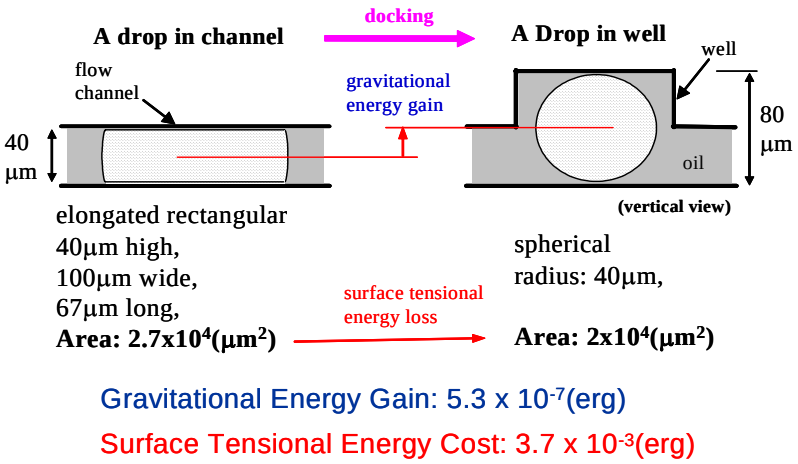

Figure 2.6. The cartoon shows that how the surface tensional energy drives the drop into the well, while it overcomes the gravitational energy gain. For simple calculation, it is assumed that the drop in the flow channel is rectangular and perfectly spherical in the well. The interfacial surface tension of water and hexadecane is 52.4(dynes/cm) [2].

2.4.2 The Fast-Slow Drop method

As shown, the preference of the docking into wells depends on the geometry of the well. It could be regulated by the height of the well. When it is deeper than twice the depth of the channel then it will remain in the well permanently, even when oil is flowing rapidly through the channel as shown in Figure 2.7a. Then, drops fill the wells in sequence with the first drop (drop #1) docking into the first empty well and the last drop (drop #2) docking into the last well. In order to stabilize the drops against coalescence the surfactant should be added so that the drops pass over filled wells without mixing. In Figure 2.7a, stable drops of water are immersed in oil of hexadecane (Sigma-Aldrich), which is mixed with Span80 (2% v/w, Sigma-Aldrich). Care must be taken to match the volume of the drop to the wells. If the docked drop is too large, it will protrude into the

channel and the next drop will dislodge it. If the docked drop is too small, a second drop will share its well. Not all oil/water drops can be stabilized. For example, we have not found commercially available surfactants that can stabilize fluorocarbon oil/water or silicone oil/water micro drops. Therefore, we have developed a method to dock drops without having to stabilize against coalescence.

When the well is shallow, comparable with the height of the flow channel, the drops pass by the wells if the drops are fast (~1.1 cm/sec) and the drops are stored in the wells when the flow stops. This type of storing method is named ‘fast-slow drop’. In the Phase Chip utilizing the fast-slow drop method, the first drop (drop #3) falls into the last well and the last drop (drop #4) falls into the first well as illustrated in Figure 2.7b. When the drop is fast, the flow of oil generates shear stresses, which drags drops out of the wells, enough to overwhelm the surface tensional force. When the oil stream stops, the drops preferentially get into the wells where are slightly deeper than the flow channel. The fast-slow drop method is necessary when a mixture of oil and surfactant, which are unable to stabilize the dispersed phase, is employed to immerse drops that are varied combinatorially.

In our experiments, mixtures of fluorinated oils (FC-43 or perfluorodecaline) and a commercial surfactant (12%w/w, Tridecafluoro-1-octanol, Sigma-Aldrich) are used. Even though the surfactant lowers the surface tension to making it easy for creating drops and slowing coalescences, it cannot completely prevent the merge of drops, which causes some mixing of drops occurs and typically the contents of about three or four adjacent drops are shared.

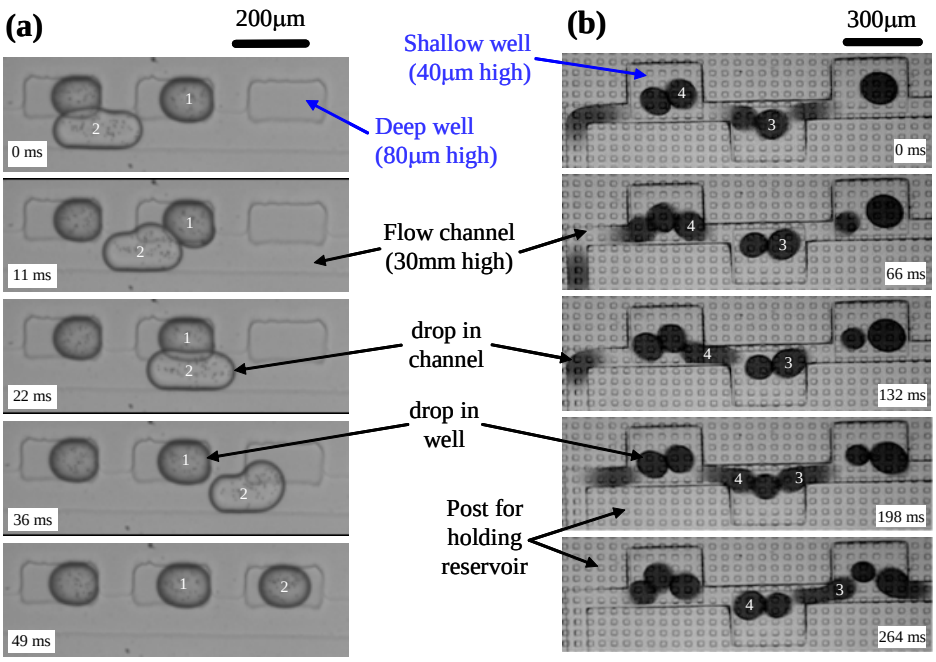

Figure 2.7. The sequence of photographs shows how drops are stored into wells. **(a)** If the height of well is deep enough (~80μm), the drops remain in wells permanently, then the second drop passes over the first drop and fall into the next available empty well. The order of drops is reversed after the docking. **(b) Slow-Fast drop**. If the height of well is shallow enough (~40μm) for the drop to pass by wells, the drops keep flowing through the flow channel. When the flow stops, each drop gets into the nearest well. The order of the drops does not change before and after the docking.

Although the experimental analysis for characterizing the fast-slow drop method was not systematically carried out, it could be speculated that the performance of the method would be better for the lower well height as long as that is higher than the flow channel. A higher flow rate of the oil could more easily dislodge the drops, and more viscous oil also generates a stronger shear stress to drag drops out of the wells.

2.5 Control of Water Contents of Stored Drops

Another significant advance of the Phase Chip over current microfluidic devices is that each well is in contact with a reservoir through a dialysis membrane, through which only water and other low molecular weight organic solvents can pass [63, 64]. Using the semi-permeable membrane, a condition in the reservoir, such as concentration or ionic strength, can be changed by replacing the fluid in the reservoir, therefore causing a change in the condition of a drop stored in well. Because the dialysis is a diffusion process, reducing dimensions by a factor of ten means decreasing the diffusion time a hundred-fold: $t = d^2/2D$ [65]. This enables the concentration of all solutes in a solution to be reversibly, rapidly and precisely varied, in contrast to current microfluidic methods developed for protein crystallization: vapor phase equilibration [4], microbatch [31], and free interface diffusion [5], which are irreversible [66].

2.5.1 The Reversible Dialysis

To perform the reversible dialysis we have developed a microfluidic device that has a thin PDMS membrane slightly permeable to water [52, 67-70], but no salt or protein is permeable. The membrane is located on the bottom of the well as shown in Figure 2.8. The membrane separates the solution from a reservoir used to establish the chemical potential to the well. Water diffuses across the membrane until the chemical potential of the reservoir and the solution in the wells are equal.

Aqueous solutions of a chemical potential that differs from that of the well can be circulated through the reservoir. When dry air, or a concentrated salt solution, is introduced into the reservoir, water permeates from the stored drops through the

membrane and into the reservoir. If pure water is introduced in the reservoir, then the chemical potential gradient is reversed and water penetrates the membrane from the reservoir into the drop, thereby diluting PDMS insoluble solutes as drops swell.

The Phase Chip has valves to control the stream of drops. In order to build the microfluidic valve, the multilayer soft lithography is used as explained in Chapter 2.3.2. The valve layer is comprised of the flow channel to carry the drops, the control channel to introduce the pressure, and the PDMS membrane in between them. It is the membrane to build the chemical potential of the reservoir and wells. So, the dialysis membrane and the valve membrane are fabricated simultaneously. Details on the manufacturing condition and processes of the valve can be found in Chapter 2.6.

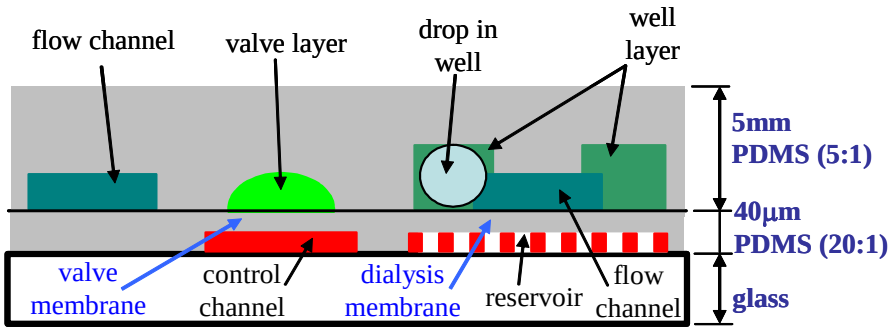

Figure 2.8. The vertical schematics of components in the Phase Chip. Reservoir and the control channel are located 15 μm below the storage wells separated by a PDMS membrane that are permeable to water. The valve and dialysis membrane are manufactured in a same process.

2.5.2 Controllability of the Reversible Dialysis

The solution stored in a well has contacts with the thick PDMS above, the dialysis membrane below and oil surrounding the drop, as shown in Figure 2.8. Are concentrations of solutes really controllable when a fluid is introduced into the reservoir

to control the water contents of the drop in this environment? What if oil surrounding a drop takes too much water? What if the thick PDMS absorbs water too quickly from the drop? In order to ascertain that the Phase Chip has the controllability over the water contents of the drop, an experiment was performed.

The device in Figure 2.9 contains two types of wells holding aqueous drops. One type of well contains a drop (#1) that is separated vertically from the reservoir by a 15μm thick PDMS membrane. Another type of well has a drop (#2) that is sitting 100 μm away horizontally from the reservoir. Initially, all drops in the device are the same size, as in Figure 2.9a. The solution of 0.5 M sodium chloride is stored in the well to set the chemical potentials between wells and the reservoir.

In Figure 2.9b, when air is introduced into the reservoir, the water transports from the stored drop, and diffuses through the thin PDMS membrane into the dry air. The drop (#1) stored in the inner well shrinks a lot, however, the drop (#2) stored in the outer well shrinks a little because the reservoir is too far away to effect it. The absorption of water by the thick PDMS layer mostly shrinks the drop (#2). Therefore, the drop in the outer well keeps shrinking even if the chemical potential is reversed by circulating the pure water through the reservoir, while the drop in the inner well swells, as illustrated in Figure 2.9c. The diameter of the drop in the inner well comes back to its initial size in 15 hours. Although the thick PDMS layer also continues removing water from the drop (#1), the chemical potentials set by the reservoir removes or adds enough water through the PDMS membrane to reversibly control the water content of the drop stored in the inner well.

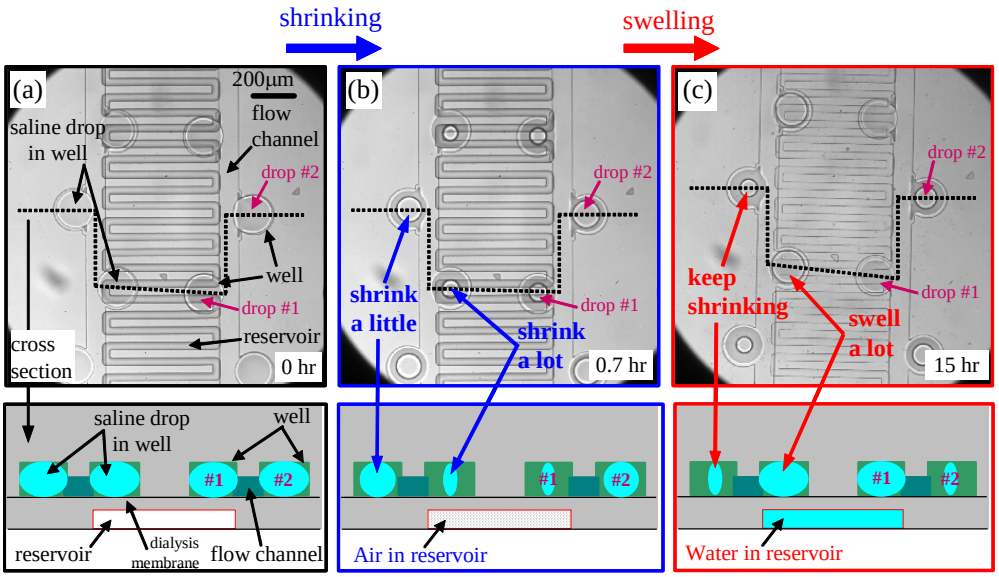

Figure 2.9 (a) Initial drops stored in the well. There are two kinds of wells; one is sitting on the reservoir through a 15 μm membrane and the other is 100 μm away from the reservoir. **(b)** After shrinking with the dry air in the reservoir, the drop (#1) is a lot smaller than the drop (#2). **(c)** When circulating water in the reservoir, the drop (#1) comes back to its initial size while the drop (#2) keeps shrinking. The diameter tracking of the drop reveals the reversible dialysis through the thin PDMS membrane is a dominant control to conduct concentrations of the drop stored in the well, rather than the absorption of water by the thick PDMS layer or an evaporation of water to oils.

In this fashion, concentrations of the stored drops are controllably varied. This experiment demonstrates that diffusion through the thin PDMS membrane is the mechanism governing drop size, not volatilization of the drops into the carrier oil or bulk PDMS device. The systematic analysis of water permeations in the Phase Chip is discussed in Chapter 3. The analysis is based on the assumption of the planar one dimensional diffusion through the PDMS membrane and the thick PDMS layer above the stored drop. Although the water is slightly permeable to fluorinated oils, the analysis

neglects the solubility of water into the oil. The shrinking rates of water into a number of fluids are discussed in Appendix 2.1. And, the method for measuring thicknesses of the PDMS membrane is explained in Appendix 2.2.

2.6 Characterization of Microfluidic Valves

This chapter will explain how to fabricate valves to control the stream of drops. The Phase Chip is a multilayer device, which means the device is composed of at least 2 different PDMS layers. As shown in the schematic diagram of the device's vertical structure (Figure 2.10b), there are the flow channel in the thick upper PDMS layer and the control channel in the thin bottom layer. This multilayer structure is built utilizing "multilayer soft lithography" as explained in Chapter 2.3.2, which combines soft lithography with the bonding of multiple PDMS layers; while each layer is cast from its own master.

When pressure is introduced into the control channel, the PDMS membrane, being just 15 μm thick (refer to Appendix 2.2) and of very soft material with Young's modulus ~250kPa [71], easily deflects upward to seal off the flow channel allowing large deflection with little force. So, the performance of a monolithic valve depends on the dimensions of the crossing between flow and control channels, as well as the depth and vertical profile of the flow channel. The recommended geometric ratio of the width and height of a flow channel is known to be 10:1 [61], and the round (hemi cylindrical) flow channel has better sealing ability than the rectangular one [3].

2.6.1 Experiment for Optimizing Valves

In order to obtain the proper dimensions for valves, a mask is designed to test a number of different pattern widths as shown in Figure 2.10a. The six parallel flow channels, running vertically, are made out of positive photoresist (AZ PLP 100XT, Clariant) varying from 100 μm to 500 μm. Once developed, positive photoresist patterns are heated above the glass transition temperature (125 ˚C for 5 minutes) and photoresist patterns reflow into round cross-sectional channels. The six parallel control channels with varying widths (100 μm to 600 μm) are made out of the negative photoresist (SU8-2025, Microchem Inc., MA) that is a thermosetting resin, which is impossible to melt, and so the control channel keeps its rectangular cross-section. The method and recipe of the multilayer soft lithography are described in Chapter 2.3.

In Figure 2.10a, the red channel represents the flow layer; the blue channel represents the control layer. At the top of the red layer, water drops form at the T-junction nozzle into the continuous phase: hexadecane mixed with 2%w/v Span80 (Sigma-Aldrich). If pressure is not introduced into the control layer, the flow channels stay open and the stream of drops keep flowing out of the device through the 1st exhaust, even if the 2nd exhaust is always open. Because the 2nd exhaust has a very long serpentine channel generating at least 5.4 times more hydrodynamic resistance (~L/D^3 with L the length, h the height [6]) than that of the 1st exhaust, the drops predictably flow out through the 1st exhaust. If the flow channel is tightly sealed off under the application of pressure through the control channel, the hydrodynamic resistance to the 1st exhaust increases infinitely. The stream of drops can overcome the flow resistance from the 2nd exhaust and begins to flow out through the serpentine channel.

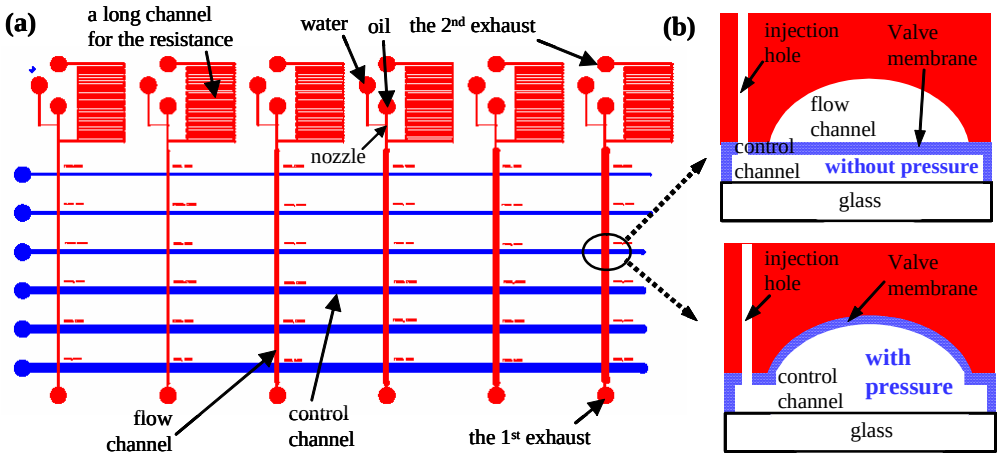

Figure 2.10 (a) The design of the test device for estimating the dimensions of valves. The widths of the control channel are 100 μm, 200 μm, 300 μm, 400 μm, 500 μm and 600 μm, which have rectangular cross sections, and the height is 30 μm. The widths of the flow channel are 100 μm, 150 μm, 200 μm, 300 μm, 400 μm and 500 μm, which have rounded cross section to enhance the performance of valves [3], and its height is 40 μm. The water drops form at the nozzle into the continuous phase. When the pressure is not introduced into the control channel, the valve membrane is flat (the upper cartoon in (b)), allowing the drops flowing out through the 1st exhaust. When pressure is applied, the membrane deflects up to close off the flow channel, switching the drop flow into the 2nd exhaust (the lower cartoon in (b)). **(b)** The schematic vertical structures of the junction of the flow and control channel. The flow channel is in the upper thick layer and the control channel is in the bottom thin layer. The PDMS slab is attached to the glass substrate permanently by an oxygen plasma treatment.

Switching of the drop stream is visually determined while applying the pressure to the control channel using a 5 ml volume syringe. Estimation of the pressure is made by measuring the volume of air in the syringe before and after the switching. The actuation pressure is calculated with the ideal gas equation $pV = nRT$ with p the pressure, V the volume change before and after the switching, n the quantity of air, R the gas constant, and T the temperature. Because nRT is identical for before and after the pressure

application, the final pressure is estimated; $p_2 = p_1 V_1 / V_2$ with p_2 the applied pressure, V_2 the final volume, p_1 the atmosphere pressure and V_1 the initial volume.

2.6.2 Results

As shown in Figure 2.11, the actuation pressure applied to switch the stream of the drops is monotonically decreasing with respect to the increasing of the width of the channels. This is in good agreement with a literature [3]; however, Figure 2.11c shows abnormal increasing of the actuation pressure when the width of the flow channel is wider than the 300 μm in case the control channel is narrower than 200 μm. This is probably due to the limited flexibility of the PDMS membrane. When the control channel is 100 μm narrower than the control channel, it needs a higher pressure to deflect up and close the wide flow channel.

In order to design microfluidic devices, one will need to fit all design parameters into the limitation of the experiment's apparatus. The limitation is the pressure in case of designing valves. In the experiment setup, the small solenoid valves, which are electrically controlled by the LabView (National Instrument Inc.), are used to apply the actuation pressure into the control channel. The solenoid valve (HDI 3-way solenoid valve, The Lee Company, CT), employed in my experimental setup, is able to handle up to 15 psi. In order to obtain the proper operation of microfluidic valves, the control channel have to be wider than 200 μm, and the flow channel should be wider than 150 μm. The dimensions of control and flow channels are extracted from Figure 2.11b-c respectively. However, if the channels are too wide, the PDMS membrane is not able to hold its structure. The valve membrane collapses permanently to the bottom of the

control channel or to the top of the flow channel. So, The width of the channel should be determined accordingly.

Typically, the 400 μm width control channel and the 300 μm flow channel are used in the Phase Chip. The photographs in figure 2.11d-e show that valves are switching the stream of water drops. The color in the crossing of the layers is orange when the valve is closed because the deflection of the membrane push the fluid in the flow channel out, and fill the control channel with the solution with a orange coloring.

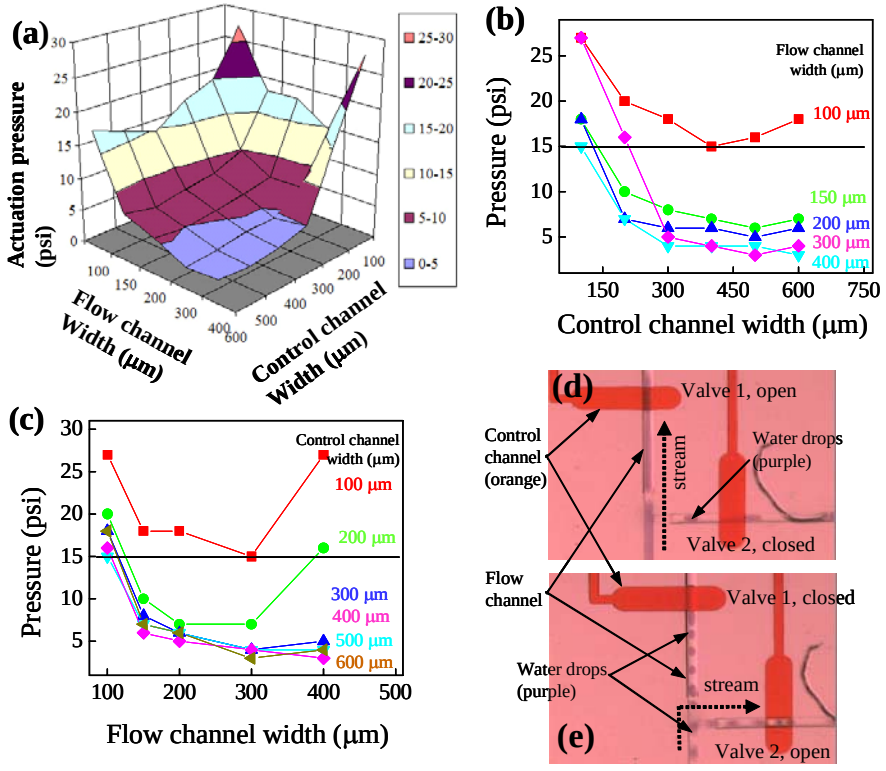

Figure 2.11 (a) The 3D plot of the actuation pressure vs. channel dimensions. **(b)** The x-y plot of pressure vs. control channel widths. Each symbol represents the flow channel with a different width. **(c)** The x-y plot of pressure vs. flow channel widths. Symbols represent widths of flow channels. To properly design valves, channel dimensions should be chosen below 15 psi of pressure (solid line). **(d),(e)** Photographs of valve operations. They show that the switching of the stream with respect to the status of valves.

2.7 Surface Treatments on the Flow Channel

The PDMS is a superior material to fabricate the microfluidic device for use with the chemical and biochemical applications in aqueous solution. It is easy to handle, transparent for optical observations, and has a low manufacturing cost. However, the PDMS has some problems in practical use. One is its incompatibility with organic solvents [51]. Many organic solvents can swell the material, causing disruption in micron size features [72]. Even water is slightly permeable to PDMS although it is a naturally hydrophobic material [69]. The other is the possibility of the adsorption of biochemical reagents [73].

2.7.1 Water Sticking on PDMS

We found drops of protein solution sticking to the surface of microfluidic channels made out of PDMS, as shown in Figure 2.12a. Once the protein drops begin to coalesce on the surface, the following aqueous drops passing over the location merge and re-break. More seriously pure water drops begin to stick to the surface of the PDMS channel after water has been flowing through it for 1~2 hours.

The mechanism of the aqueous drop sticking is not well understood. It could occur due to adsorption of chemical reagents on the surface, or as a result of contaminated surface of the channels with contaminants, since the sticking does not occur throughout the device. Figure 2.12a shows that a temporal sequence of the merging of protein drops onto the specific location in the flow channel. Once the coalescence of drops occurs, it is very difficult to flush the source of merging out of the channel, and the region where drops

merge even spreads along the flow channel. Thus, the manipulating drop fails and the merging of subsequent drops causes concentrations in the drops smeared out.

2.7.2 CYTOP

In order to overcome this sticking problem, the extra thin film is coated on the surface of the microfluidic channel made out of PDMS. The film should satisfy some requirements. It is necessary to form a reliable layer on surfaces, which is exposed to solvents, without clogging the channel. The coated film has to provide a very effective covering to keep solvents and solutes away from the channel wall. And, it should adhere strongly to PDMS. There is a commercially available fluorocarbon polymer, which is able to coat on the PDMS surface. It is CYTOP (Asahi Glass Company). Kanai et al used CYTOP to passivate the surface of the PDMS [73].

CYTOP-107M is a perfluoro-polymer, which is a coating material consisting of 7 %(w/w) solution of poly (1,1,2,4,4,5,5,6,7,7,-decafluoro-3-oxa-1,6-heptadiene) (molecular weight 60,000 ~ 70,000) dissolved in CT-solv100 (perfluorotributylamine). The molecular structure of CYTOP is shown in Figure 2.12b. The glass transition temperature of CYTOP is 108 ˚C, and the boiling point of the solvent is 100 ˚C. CYTOP film on the PDMS channel doesn't interrupt the visual observation because the transmittance is more than 95 % for 200 μm thick film in the frequency range of 400 nm ~ 700 nm. Also, the substrate doesn't require pre-treatment for direct adhesion onto metal, silicon, silicon oxide, silicon nitride and glass. As the PDMS is a silicon-based organic material [60, 74], CYTOP can directly adhere to the surface of the PDMS.

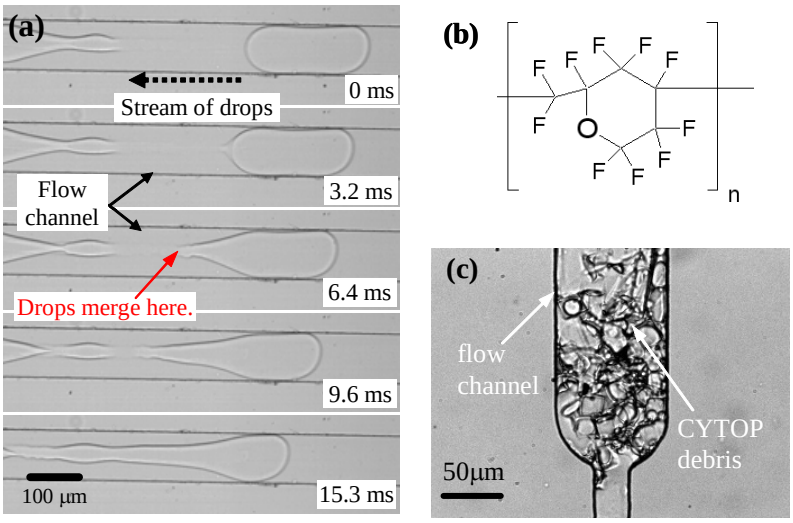

Figure 2.12 (a) The sequential photographs show the protein drops are merging on the surface of the microfluidic channel where the protein is probably adsorbed on. The protein solution is about 40 mg/ml of lysozyme (Seikugaku) in the buffer of sodium acetate 0.1 M, pH 4.5. The oil is FC-43 (3M) with the surfactant (5%wt of Tridecafluoro octanol, Sigma-Aldrich). **(b)** The molecular structure of CYTOP perfluoro-polymer. It is coated on the surface of the channel by the multi step process. It can nicely keep the protein solution and water away from surfaces of the channel to prevent the permanent sticking. **(c)** The CYTOP debris is clogging the channel. If the concentration of CYTOP solution is too high (more than 0.5 %(w/w)) or the high temperature curing is not enough, CYTOP film is peeled off the surface and blocking the channel. Once the debris clogs the channel, all the following drops coalesce.

2.7.3 Process Conditions for Coating

CYTOP is coated on the surface of the flow channel by allowing it to flow through. CYTOP-107M solution comes at 7 %(w/v), and we dilute it down to 0.25 %(w/v) to form thin layers and to prevent CYTOP debris (Figure 2.12c), which are left in the channel

after curing if CYTOP concentration is too high. The following is the multi-step process to form the protection layer on the channel.

Step 1. Flowing CYTOP solution into the flow channel.

A syringe pump is employed for the injection and the typical flow rate is 30 μl/hr. As shown in Figure 2.1, the Phase Chip is a multi-junction device, which means the device is comprised of a number of regions. When CYTOP solution is introduced into the device, the solution flows out through the easiest way, which has the least flow resistance. Then the most of the regions, connected to the easiest path through a junction, won't have enough CYTOP in it. In order for the CYTOP solution to flow through the device and remain in each part for long enough for the CYTOP film to coat the surface of the channels, the counter pressure should be applied to prevent the flowing of CYTOP solution through the easiest way as shown in Figure 2.13a.

Since the CYTOP solution is forced to flow into the channels by volumetric control, the solution stay and fills all regions in the device until the pressure built in the device matches the counter pressure. When the pressure of CYTOP solution in the device overwhelms the counter pressure, the solution slowly flows out of the device while CYTOP solution fills all regions of the Phase Chip.

There is another advantage to the CYTOP solution staying longer in the channel: accumulation of CYTOP solutes on the surface. As explained in Chapter 2.8, the CYTOP solvent (perfluorotributylamine) has a relatively high permeability even though fluorinated fluids penetrate through the PDMS with a low permeability. When the solvent leaves the channel into bulk PDMS, the solutes are probably left on the surface. The

longer the CYTOP solution stays in the channel, the denser CYTOP film accumulates on the surface.

There is another way to enhance the permeation of the solvent. It is by heating. The penetration of the solvent should be accelerated at the higher temperature. So, CYTOP coating is done on the hot plate at 75 ˚C for 30 minutes because the boiling point of the solvent of CYTOP-107M is 100 ˚C. Using a higher concentration of CYTOP is an alternative way to get a denser and thicker film of the CYTOP solute. However, when the higher concentration (> 0.5 %(w/w)) of the CYTOP solution is used, the thick CYTOP debris is easily made in the channel and they clog the channel as shown in Figure 2.12c.

Step 2. Blowing CYTOP solution out of the device.

It is necessary to remove from the channel any extra CYTOP solution that is not deposited on the surface. Otherwise, CYTOP is heavily accumulated on the surface, and forms an easily breakable thick film, which causes the clogging of the flow channel. In order to remove the CYTOP solution, air is blown into the channel. The air pressure is increased up to 12 psi as long as no delamination between PDMS layers happens, as shown in Figure 2.13b. In a multi-region device like the Phase Chip, it is also hard to remove the CYTOP solution out of the device because the air finds the easiest way to get out. So, the microfluidic valves in the device are used to distribute air properly into the branch regions through junctions. This blowing out process is also done at the temperature of 75˚C.

Step 3. Curing CYTOP.

The CYTOP solution coated in device is baked at the two different temperatures after the blowing out process. Firstly, the solvents need to be evaporated. Because the boiling point of the solvent is 100 ˚C, the temperature of the 1st bake is 110 ˚C for 2 hours.

Secondly, it is necessary to glassify the CYTOP film, deposited on surfaces, to form the sturdy layer on the microfluidic channel. The glass transition of CYTOP is 108 ˚C, so the 2nd bake is done at 210 ˚C for another 2 hours.

The resulting CYTOP film is pretty reliable. The durability of the film can be briefly tested. The sticking problem has not happened even after 48 hours of flowing water drops in the fluorinated oil (FC-43, 3M). As shown in Chapter 4, the crystallization experiments have been done for 6 days. During the experiment, the protein solution continues to form beads on the surface of the microfluidic wells.

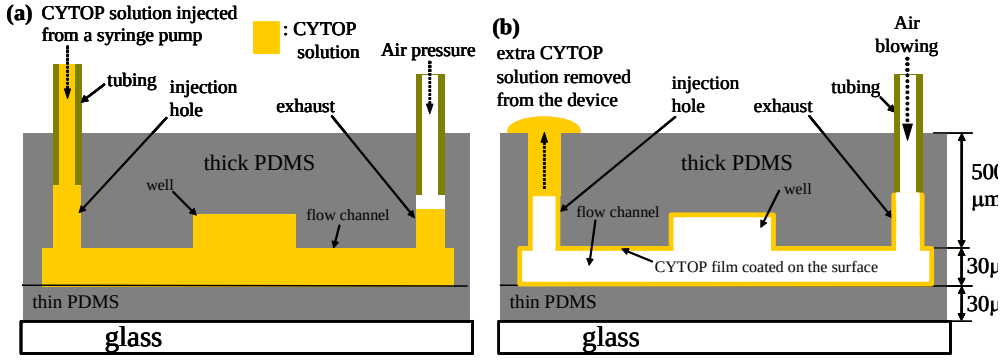

Figure 2.13 (a) A schematic cartoon shows the injection of CYTOP solution. When CYTOP is encountered into the device, the counter pressure should be always applied to stay and flow the solution into all region of the device. Otherwise, the solution is flowing out through the way having the least resistance. This process is done on the 75 ˚C hot plate to enhance the permeation of the solvent. **(b)** It is necessary to remove the extra CYTOP after the coating completes. Otherwise, CYTOP debris, if any, may cause the clogging the channel, which is a fatal problem.

2.8 Permeations of Fluids into PDMS

The fluids ran in the Phase Chip are presumably immiscible with each other; however not perfectly immiscible. The physical phenomenon with which we are concerned in this Chapter is the permeation of one fluid into another fluid.

When an aqueous drop is stored in the well, the drop is exposed to two different materials, oil and PDMS. In order to understand the reversible dialysis properly, the permeation of water into the oil and PDMS should be investigated. If the oil takes water so quickly or the thick PDMS above the drop removes water too much, the controllability of the dialysis will fail. Also, oils are able to permeate into PDMS [51, 75]. After plugging all injection holes of the Phase Chip to induce the chemical or physical reaction in stored drops we found that voids in the flow channel came out, because the PDMS absorbs oil.

In order to estimate the permeation between fluids, we measured the shrinkage rate that is defined by area changes of a drop, immersed in another liquid, as a function of time. He et al derived the shrinkage rate (dA/dt) from the diffusion equation [76]; $dA/dt = -8\pi M_w D_{wo} (C_w - C_{w-ref}) / \rho_w$ where A is the area of water drops, M_w and ρ_w are the molecular weight and density of water, D_{wo} is the diffusivity of water in a liquid, C_w and $C_{w\text{-}ref}$ are the concentrations of water on the surface of the drop and at a reference point that is far away from the drop. After the shrinkage rates of the water immersed in many different liquids are measured, the permeations of water ($D_{wo}(C_w - C_{w\text{-}ref})$) into the liquids are compared. The higher shrinkage rate represents stronger permeation. The shrinkage rates of water with respect to PDMS and oils determine which one is the dominant factor for controlling water contents of the solution stored in the well.

2.8.1 Shrinkage Rates

As illustrated in Figure 2.14a, a water drop is immersed in a liquid, contained in the Petri dish made out of glass to prevent permeation of water into the container. After the drop sinks on the bottom, the cross sectional area of the drop is measured as a function of time by taking and analyzing pictures with Image J (NIH). If the density of the liquid is less than water, water drops are immersed in the liquid. Otherwise, drops of the liquid are formed in water. After dripping the water with a micro pipette, the pipette tip is used to stir and break up the drop.

When analyzing the pictures, it is assumed that the shape of the drop is perfectly hemi-spherical. The areas of the drop are calculated with diameters estimated from cross sections of the drop. This assumption may give some errors for data analysis since the actual shape of the drop is determined by the interfacial surface tension and the surface treatment on the Petri dish. However, a possible range of the error should be within about 2 folds because a surface area of a perfect hemi-sphere is exactly half of a circle having the same diameter.

Figure 2.14b shows the shrinkage rates of water into oils and PDMS. The PDMS having 10 cSt and 100 cSt of kinematic viscosity are used for the experiment because the liquid PDMS for casting the microfluidic device is too viscous (3790 cSt) to sink water drops onto the bottom. As long as the shrinkage rate of water in an oil is lower than the rate in liquid PDMSs, the oil is usable for the reversible dialysis in the microfluidic device. The fluorinated materials; PFD (perfluorodecaline, Sigma-Aldrich), FMS-121 (Fluorosilicones, Poly(3,3,3-Trifluoropropylmethylsiloxane), Gellest) and FC-43 (Perfluorotributylamine, 3M) perfectly isolate water drops as expected.

We also measured the shrinkage rates of liquid PDMS immersed in oils (Figure 2.14b). From these data, only FMS-121 looks appropriate for the PDMS microfluidic device. But, there is a hydrodynamic limitation for FMS-121 to be employed. The viscosity of FMS-121 is too high (100 cSt) to inject the fluid into the channel. We couldn't generate water drops in FMS-121 before delaminating the multilayered PDMS device because the pressure in the channel is so strongly built up, caused by high hydrodynamic resistance.

So, as long as we tested, FC-43 is the best candidate in terms of the permeation into the PDMS and the ability to isolate aqueous drops. Figure 2.14c shows that hexadecane (Sigma-Aldrich), flowing in the flow channel, permeates through the thin PDMS membrane into reservoir, and swells the PDMS posts that hold the membrane. The hexadecane, intruded into reservoir, interrupts flowing of salt solutions, which set the chemical potential of water between the reservoir and wells.

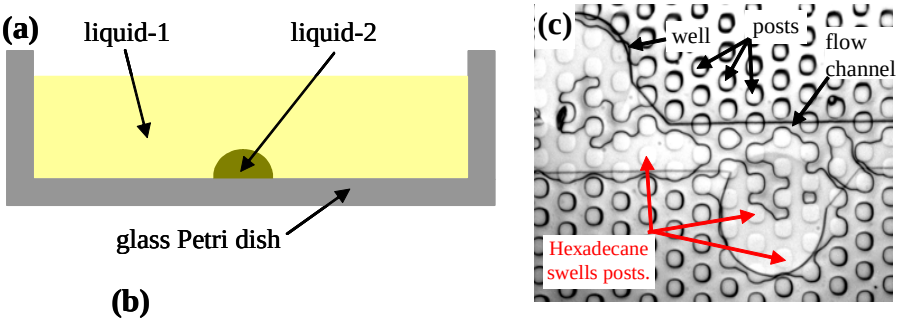

(b)

		Density (g/cm^3)	Shrinkage Rate ($\mu m^2/min$)
Water	PFD	1.94	0
	FMS-121	1.24	0
	FC-43	1.93	0
	Light Mineral oil	0.84	4.6
	Heavy Mineral oil	0.85	5.8
	Hexadecane	0.77	15
	PDMS 100cSt	0.96	46
	PDMS 10cSt	0.93	50
PDMS 10cSt	FMS-121		0
	FC-43		118
	PFD		1472
	CYTOP		2308
	Light Mineral oil		Dissolve
	Heavy Mineral oil		Dissolve
	Hexadecane		Dissolve

Figure 2.14 (a) A schematic diagram for the measurement set up. **(b)** The shrinkage rates between fluids. The data reveal that FC-43 is one of the best oil for realizing the reversible dialysis method in PDMS devices because FMS-121 is too viscous to form water drops. **(c)** A photograph shows hexadecane is permeating through the PDMS membrane.

Appendix 2.1 Measurement of the Membrane Thickness

The PDMS membrane has very important roles in the performance of the Phase Chip. The first task is as the reversible dialysis membrane, whose semi-permeability is exploited. As discussed in Chapter 3, the exchange of water occurs by the diffusion through the thin (15 μm) and wide (300 μm) PDMS membrane. In order to extract the diffusion coefficient or permeability of water in PDMS, the thickness of the membrane should be precisely measured. The diffusion equation says the flux through the membrane is proportional to the concentration difference, and inversely proportional to the thickness, $J = -D \cdot \Delta C_{water} / m$ with J the flux of water through the membrane, D the diffusion coefficient, ΔC_{water} the difference of the water concentrations and m the thickness of the membrane. The second important task is as the valve membrane. As reported in [3], the actuation pressure applied into the control channel to seal off the flow channel by the deflection of the PDMS membrane increases linearly with its thicknesses. The actuation pressure jumped 14 times when the thickness varies from 4 μm to 16 μm.

To fabricate the optimized and consistently working microfluidic device, it is necessary to monitor the membrane thickness. Studer et al measured the thickness by the optical microscope [2]. They broke a device and inspected vertical cross-sections of the membrane that is about 10 μm thick under the microscope with 100x objective lens.

We have measured the thickness of membranes in different way. We believe it is an easier and more precise method, and the device is still usable after the measurement. As shown in Figure 2.15a, the 5 %(w/w) suspension of the 1 μm diameter micro spheres (Polystyrene Micro sphere, Polysciences Inc.,) in water is injected into the flow channel.

After the device is baked on the hot plate at 85 ˚C to evaporate water, most of the spheres settle down and deposit on the bottom of flow channels and wells. And then, the reservoir is filled with the suspension of the micro sphere as in Figure 2.15b, the device is baked again on the hot plate at 85 ˚C with the device upside down. The spheres stick to the top of reservoir. The result is that there are two layers of micro spheres above and below the membrane.

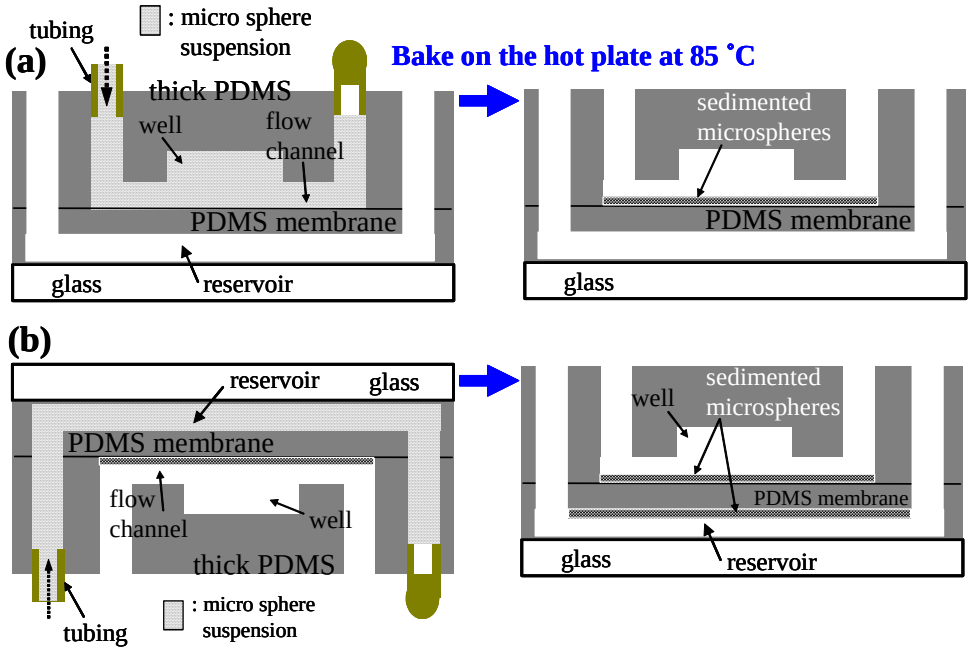

Figure 2.15. The sedimentation of the micro spheres **(a)** on the bottom of wells, **(b)** on the top of reservoir. In order to speed up evaporations of water, the device is baked 85 ˚C. After all, the most of the spheres are sitting on the bottom and sticking on the top.

The membrane thickness is measured under the microscope (Inverted Microscope, Nikon) by adjusting the focus. Because of the narrow depth of field of the high magnification objective lens (20x), the micro spheres sitting on the bottom of the wells could be in focus while the spheres sticking on the top of reservoir are out of focus. By

changing the focus from the spheres sitting on the bottom to the spheres sticking on the top, the thickness of the membrane can be measured. There is a ruler on the focus adjustment knob in the microscope to read the height of the objective lens. Since the depth of field of the 20x objective lens is 5.8 μm [40] and the diameter of the micro sphere is 1 μm, the measurement error is approximately within 3 μm.

The membrane thickness depends on the spinning speed when the liquid PDMS, which is 5:1 weight ratio of pre-polymer and crosslinker, is coated on a master. For the recipe of 2500 rpm/60 seconds, the average thickness is 15 μm, and for 700 rpm/90 seconds, the thickness is 39 μm.

Chapter 3

Understanding Water Transport and Control of the Phase Behavior of Aqueous Solutions in the Phase Chip

3.1 Overview

The Phase Chip is able to controllably vary the water content of the docked drops. As illustrated in Figure 3.1, this is accomplished by fabricating the bottom of the wells from a thin PDMS membrane (15 μm thick) that is slightly permeable to water [69, 70], but impermeable to proteins, poly(ethylene glycol) (PEG), and salts. The other side of the membrane contains a 100 nano-liter reservoir, through which flows either dry air or an aqueous salt solution. This produces a chemical potential gradient between the solution stored in the well and the reservoir.

When the reservoir is filled with dry air or a solution whose salt concentration is greater than that of the drop then water permeates from the stored drops in the wells through the membrane into the reservoir thereby increasing the concentration of the

PDMS-impermeable solutes inside the drop. If, in contrast, pure water is introduced in the reservoir, then the chemical potential gradient is reversed and water permeates the membrane from the reservoir to the drop, thereby diluting each PDMS-impermeable component as the drops swell. Because the drops stored in the wells are confined in one dimension, they have a disk-like shape so that when the drops shrink and swell, only the area of drops change, not the height.

This chapter describes the permeation of water in the Phase Chip, which can be modeled using the diffusion equation, resulting in a good agreement between experiment and theory. In addition, it shows that the phase diagram of a polymer/salt mixture can be measured employing the Phase Chip, which also agrees well with the phase diagram obtained off-chip.

3.2 Understanding Water Transport in the Phase Chip

As shown in Figure 3.1, there are two paths through which the water permeates the Phase Chip; the principal one is through the thin PDMS membrane separating the wells and the reservoir, and the secondary one is a leakage path through the thick PDMS above the wells to the exterior of the device. The flux of water along each of these paths is $J_i = -P\nabla c_i$ with $P = kD$ where P is the permeation coefficient, $k = 7.1\times10^{-4}$ and $D = 8.5\times10^{-10}[\mathrm{m}^2/\mathrm{s}]$ are the solubility and diffusion constant of water in PDMS [69, 70], respectively, and ∇c_i are the gradients in water concentration along each path.

The flux of water between the drop and reservoir through the thin PDMS membrane can be considered as 1-dimensional planar diffusion as the disk-shaped drops have a typical diameter of 300 μm and height of 30 μm, while the thickness of the membrane is

15 μm. Furthermore it is assumed that the flux of water through the thick PDMS is also planar diffusion. The reservoir has several basic designs. One consists of a series of serpentine, parallel channels. Because the channels are separated by a distance (200 μm) small compared to the thickness of the entire PDMS device (5000 μm) and the linear dimension of the channels is much greater than the thickness of the PDMS device it is valid to approximate diffusion between the wells and exterior of the device as planar diffusion.

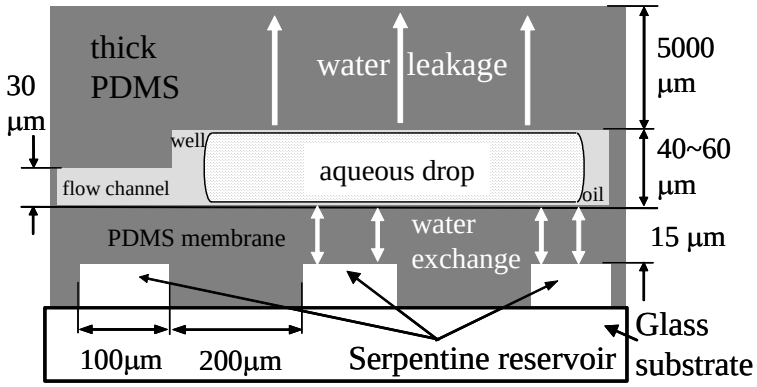

Figure 3.1 Schematic vertical structure of the Phase Chip. Aqueous drops of sodium chloride solution are stored in wells. In the upper, thick (5 mm) layer, there are flow channels and storage wells. In the lower, thin (40 μm) layer, there is a reservoir, sealed by a 15 μm thick PDMS membrane. The principle path for water flux is between the drop and the reservoir, but there is a small leakage flux through the 5 mm thick PMDS layer between the drop and the device exterior.

3.2.1 One Dimensional Diffusion Theory

The gradient of water concentration across the thin PDMS membrane separating the drop and the reservoir is $\nabla c_{res} = \Delta c / m = (c_{drop} - c_{reservoir}) / m$ while the gradient in the water

concentration between the drop and the exterior of the device is $\nabla c_{\text{ext}} = \Delta c / M$ $= (c_{\text{drop}} - c_{\text{exterior}})/M$ with c_{drop}, $c_{\text{reservoir}}$ and c_{exterior} the concentrations of water in the drop, reservoir, and the exterior of the device respectively, while *m* is the thickness of the PDMS membrane separating the drop and reservoir and *M* is the thickness of the PDMS separating the drop and the exterior of the device. The molar concentration of water can be expressed in terms of the molar concentration of solutes as $c_\alpha = W - X_\alpha$ where α indicates either the drop, reservoir, or external environment, W = 55 M is the molar concentration (mol/liter) of pure water, and X_α is the molar concentration of solute, such as salt or PEG. Thus $-\nabla c_{\text{res}} = (X_{\text{drop}} - X_{\text{res}})/m$ and $-\nabla c_{\text{ext}} = (X_{\text{drop}} - X_{\text{ext}})/M$. Usually the water concentration exterior to the device is zero, $c_{\text{exterior}} = 0$, or equivalently X_{ext} = 55 M.

The total molar flux (J (m M s^{-1})) of water out of the drop is $J = -P \cdot \nabla C_{\text{water}}$ $= kD \cdot \left((X_{\text{drop}} - X_{\text{res}})/m + (X_{\text{drop}} - X_{\text{ext}})/M \right)$. Assuming that only water and not the solute permeates the PDMS allows relating the volume change of the drop to the molar flux of water from the drop as $dV/dt[\text{m}^3\text{s}^{-1}] = h \;\; dA(t)/dt = J \;\; A(t)/W$ with $V[\text{m}^3] = A(t) \cdot h$ being the volume of a drop, *A(t)* the area of the drop and *h* the constant height of the confined, disk-shaped drop. Since only water leaves the drop, the concentrations of solutes in the drop are inversely proportional to the drop's volume, thus the solute concentration of the drop as a function of time is $X_{\text{drop}} = X_{\text{o}} \cdot V_{\text{o}}/V(t) = X_{\text{o}} \cdot A_{\text{o}}/A(t)$ with V_{o}, A_{o}, and X_{o} the initial volume, area and concentration of a drop, respectively. The resulting differential equation derived from the 1-dimensional diffusion equation and the mass conservation is $dA(t)/dt = J \;\; A(t)/(h\,W) = kD/hW \cdot \left\{ \left(A_{\text{o}} \cdot X_{\text{o}} - A(t) \cdot X_{\text{res}} \right)/m + \left(A_{\text{o}} \cdot X_{\text{o}} - A(t) \cdot X_{\text{ext}} \right)/M \right\}$.

The question we ask is how does the area of an initially equilibrated drop of area A_o and solute concentration X_o that is placed in contact with a reservoir and exterior environment of constant solute concentration X_{res} and X_{ext}, respectively, at time $t = 0$ evolve with time. The solution of this differential equation, expressed as the dimensionless relative drop area is

Equation (1) $$\frac{A(t)}{A_o} = \alpha + (1-\alpha)\, e^{-t/\tau} \;;$$

where α is the ratio of the final area to the initial area, or equivalently, the ratio of the initial solute concentration to the final solute concentration;

Equation (2) $$\alpha = \frac{A(\infty)}{A_o} = \frac{X_o}{X_\infty} \quad \text{with} \quad X_\infty = \frac{X_{res} M + X_{ext} m}{M + m},$$

and τ^{-1} is the equilibration rate of the drop;

Equation (3) $$\frac{1}{\tau} = \frac{kD}{hW}\left(\frac{X_{res}}{m} + \frac{X_{ext}}{M}\right).$$

3.2.2 Water Permeation through PDMS

Figure 3.2a shows the normalized areas of the stored drops as a function of time. Firstly, drops are equilibrated by filling the reservoir with the same salt concentration as the drops. Then the reservoir is filled with a salt solution of a different concentration. If the reservoir is filled with a higher (lower) salt concentration than the equilibrated drops, then the drops will shrink (swell). The color dots in Figure 3.2a are measured data. Each curve was fitted to Equation (1) and the parameters α and τ were extracted. In Figure 3.2b the fitted values of α (α_{exp}) are compared with the theoretical values of

α (α_{theory}) given in Equation (2). As all the parameters in α_{theory} are known, there are no free variables and within experimental variation of 5 % there is excellent agreement between our model and experiment. In Figure 3.2c the fitted rate τ^{-1} is plotted vs. the theory given in Equation (3).

All the parameters except the permeation coefficient $P = k\,D$ are measured. The proportionality between τ^{-1} and $\frac{1}{hW}\left(\frac{X_{\text{res}}}{m}+\frac{X_{\text{ext}}}{M}\right)$ as predicted by Equation (3) is observed in Figure 3.2c. The proportionality constant is found to be $P=kD = 7.4\times10^{-13}[\text{m}^2/\text{s}]$, which is consistent with literature values [69]. This agreement between theory and experiment further validates our model. In Figure 3.2a the solid lines are not fit to the data, but are the theory with only one fitted parameter for nine different experiments. The solid lines are plotted with Equation (1) for each of the nine experiments using different values of the salt concentration of reservoir and drop and constant values of the device parameters (h = 40 μm, m = 15 μm, M = 5 mm, X_{ext}= 55 M, W = 55 M, X_{res}, X_{o}) and the one fitted parameter, $P = k\,D = 7.4\times10^{-13}[\text{m}^2/\text{s}]$.

For practical applications it is useful to know how quickly the concentration of a drop is changed. The maximum rate of change, τ_{max}^{-1}, for an exponential process is the initial rate found by expanding Equation (3) for $t << \tau$; $A(t)/A_{\text{o}} \sim 1 + t/\tau_{\text{max}}$ with

Equation (4) $$\frac{1}{\tau_{\text{max}}} = \frac{\alpha - 1}{\tau} = \frac{kD}{hW}\left(\frac{X_{\text{o}} - X_{\text{res}}}{m} + \frac{X_{\text{o}} - X_{\text{ext}}}{M}\right).$$

In our experiment we use NaCl salt solutions in the drop and in the reservoir. The saturation concentration of NaCl is about 6 M, which sets the range of values of the salt concentration of the drop to be $0 \le X_{\text{o}} \le 6$. The reservoir can contain salt solutions of

this range, or contain air, which has an equivalent salt concentration of 55 M. Therefore $0 \le X_o - X_{res} \le 55[\mathrm{M}]$ while $-55[\mathrm{M}] \le X_o - X_{ext} \le -49[\mathrm{M}]$, and the gradient in salt concentration between the drop and reservoir ranges from $0 \le \frac{X_o - X_{res}}{m} \le 3.7[\mathrm{M}\,\mu\mathrm{m}^{-1}]$ while the gradient in salt concentration between the drop and exterior of the device ranges from $-0.011 \le \frac{X_o - X_{ext}}{M} \le -0.0098[\mathrm{M}\,\mu\mathrm{m}^{-1}]$. The Phase Chip is designed such that the reservoir flux will primarily set the final concentration of the drop, with the leakage flux to the exterior of the device being a small correction. In order to test whether or not the gradient in salt concentration between the drop and reservoir is controlling the drop concentration we plot the initial rate of change of the area of the drop, $\tau_{\max}^{-1}$, as a function of $X_o - X_{res}$ in Figure 3.2d. The initial rates are calculated as $\tau_{\max}^{-1} = (\alpha - 1)/\tau$ where α and τ^{-1} are obtained from fits to the data as in Figure 3.2b-c.

As shown in Figure 3.2d, the initial rates and the versus $X_o - X_{res}$ is well approximated by the linear function: $\tau_{\max}^{-1} = a(X_o - X_{res}) + b$. Fitting the slope of the line in Figure 3.2d to Equation (4) yields, $a = kD/mhW = 0.078\left(\mathrm{M}^{-1}\mathrm{hr}^{-1}\right)$ from which the permeability of water in PDMS is calculated, $P = 7.2 \times 10^{-13}[\mathrm{m}^2/\mathrm{s}]$, similar to the value we obtained from fitting only τ^{-1} in Figure 3.2c, while the intercept yields the leakage flux rate $b = \frac{kD}{hW}\left(\frac{X_o - X_{ext}}{M}\right) = -0.026\,[\mathrm{hr}^{-1}]$. As discussed previously the fact that the flux of water from the reservoir dominates the leakage flux allows us to approximate the leakage flux as a constant and treat the reservoir flux as the independent variable.

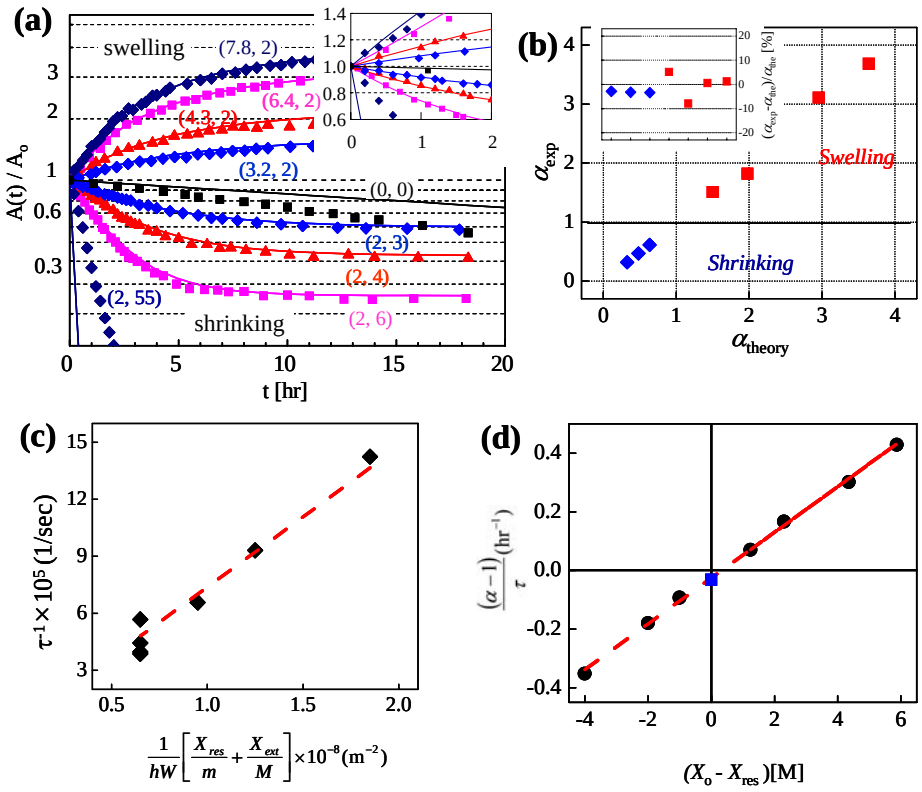

Figure 3.2 (a) The relative areas of saline drops $(A(t)/A_o)$ stored in wells with respect to time (t). Note that the vertical axis is logarithmic scale. The numbers next to each curve represent the salt concentration initially in the drop and in the reservoir (X_o, X_{res}). The black squares represent the pure leakage flux condition with the drop and reservoir containing salt-free water (0, 0). The solid lines are the theory with no adjustable parameters. The largest discrepancy between experiment and theory occurs when air is in the reservoir (0, 55). **(b)** The ratio of final to initial drop area for experiment vs. theory. The experimental values (α_{exp}) are obtained by fitting the data of (a) to Equation (1). The theoretical values (α_{theory}) are obtained using Equation (2) and the known experimental parameters. **(c)** The rate of change of the drop area, τ^{-1}, is plotted vs. $1/hW \cdot (X_{res}/m + X_{ext}/M)$. The experimental values (τ^{-1}) are obtained by fitting the data of (a) to Equation (1). Equation (3) predicts that this is a line whose slope is $P = k\,D$. **(d)** The initial rate of change of the relative area, τ_{max}^{-1}, as a function of $X_o - X_{res}$.

The interpretation of the data in Figure 3.2d is that the initial rate of change of concentration of the drop, τ_{max}^{-1}, varies linearly with the difference in concentration

between the drop and reservoir. For example, with a four molar initial difference in salt concentration between the reservoir and drop, the drop concentration will initially change by 30 % per hour. When the drop and reservoir are initially set to have the same salt concentration, the drop will still increase concentration at a rate of 2.6 % per hour due to the leakage path to the exterior of the device. The drop will not change volume if the drop contains a salt solution that is about 0.33 M more concentrated than the reservoir solution then because the flux to the reservoir is balanced by the leakage flux to the exterior of the device. If we make the more extreme approximation of ignoring the leakage flux altogether, or set $M \to \infty$ in Equation (4), we find $\tau_{\max}^{-1} = \frac{kD}{hWm}\left(X_{\mathrm{o}} - X_{\mathrm{res}}\right)$. This predicts that Figure 3.2d will be a straight line with zero intercept, which is not a bad approximation when $\left|X_{\mathrm{o}} - X_{\mathrm{res}}\right| > 1[\mathrm{M}]$.

As mentioned previously the solid curves in Figure 3.2a are not fitted to the experiment, but rather to the theory with all the parameters set by experiment. There are seven curves for which the theory and experiment have excellent agreement, corresponding to when the difference $X_{\mathrm{o}} - X_{\mathrm{res}}$ is large. The other two curves show significant deviations from theory. One (black squares) is for the case when $X_{\mathrm{o}} - X_{\mathrm{res}} = 0$. In this case the only flux out of the drop is the leakage flux. The drop concentration does not follow an exponential time variation very accurately indicating that the 1-dimensional planar approximation for the leakage flux is not as good as for the flux to the reservoir. The planar approximation underestimates the experimental leakage rate by a factor of 2 to 3. However, most of our experiments are done in a regime where the leakage flux is small compared to the reservoir flux and the planar approximation corrects for the leakage to first order. A more extreme approximation is to ignore the leakage completely in the theory, which is done

by considering the device to be infinitely thick and setting $M \to \infty$ in Equations (2) and (3). Then the final experimental concentrations, X_∞, are predicted to equal the reservoir concentration, X_{res}. Instead, as shown in Figure 3.3b the measured value of X_∞ is found to be about 5% higher than X_{res} when $|X_o - X_{\text{res}}| > 1[\text{M}]$. These systematic offsets are caused by the unidirectional feature of the leakage flux; water always flows from the drop to the exterior of the device while the reservoir can either source or sink water from the drop.

The other curve that shows deviation from theory is for the case of when the reservoir contains dry air. In this case the concentration of water in the reservoir is zero and we consider this equivalent to filling the reservoir with a salt solution of $X_{\text{res}} = 55[\text{M}]$. In the experiment air is driven through the 30 μm deep reservoir by applying a pressure of 10 psi. The data shows that the rate of drop shrinkage is much slower than predicted. We speculate that this is due to the air forming a stagnant boundary layer inside the reservoir and that if the reservoir was deeper, or the air flowed faster then a faster shrinking rate would be obtained.

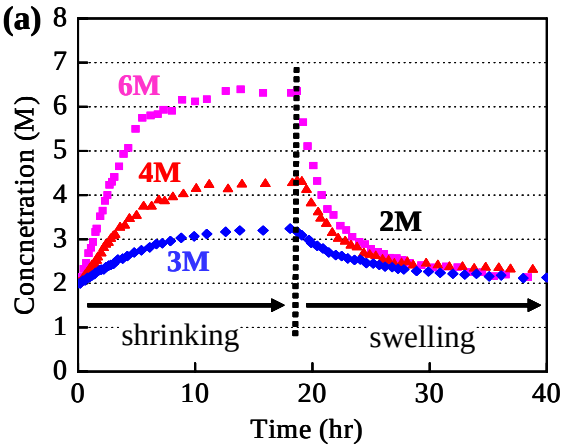

(b)

		■	▲	◆
Initial concentrations of drop [M]		2	2	2
Shrinking drops	Reservoir concentration while shrinking [M]	6	4	3
	Experimental concentrations after shrinking [M]	6.4	4.3	3.2
	Theoretical concentration after shrinking [M]	6.15	4.15	3.16
Swelling drops	Reservoir concentration while swelling [M]	2	2	2
	Experimental concentrations after swelling [M]	2.1	2.2	2.1
	Theoretical concentration after swelling [M]	2.16	2.16	2.16

Figure 3.3 (a) The concentration of saline drops stored in wells with respect to time. Concentrations are determined by measuring the drop area: $X_{drop} = X_o \cdot A_o / A(t)$. The data is identical to Figure 3.2a. All drops had the same initial sodium chloride concentration, X_o = 2 M, and at $t = 0$ are exposed to different reservoir conditions (X_{res}) for 18 hours: 6 M (pink square), 4 M (red triangle), 3 M (light blue diamond). Next the reservoir conditions are all changed to the same condition; X_{res} = 2 M, the initial condition of stored drops. **(b)** The table shows the equilibrium drop concentrations obtained by fitting Equation (1) to the data in (a) to obtain α and thus the experimental concentration while the theoretical value for α is calculated from Equation (2).

3.2.3 Salt Permeation through PDMS

A central assumption of our model is that only water and not any of the solutes permeates through the PDMS membrane. Figure 3.3 demonstrates that this is the case for sodium chloride (NaCl), which shows the time evolution of the concentration of drops containing NaCl solution as a function of reservoir concentration.

The initial NaCl concentration in the drops was 2 M and the reservoir was filled with a greater NaCl concentration (3 M, 4 M, and 6 M) than the initial drop concentration. In these cases water leaves the drop, which shrinks in volume. For these conditions it takes approximately 15 hours for the drops to equilibrate. Once equilibrated, the reservoir concentration is replaced with 2 M of NaCl solution. This reverses the chemical potential difference between the reservoir and drop causing water to be transported from the reservoir to the drops. In response the drops swell until equilibration is established.

We assume that none of the salt leaves the drop during the forty hour experiment. The final measured drop volume implies a final salt concentration slightly larger than that in the reservoir (2.1 M ~ 2.2 M), which is exactly what is predicted by Equation (2). Since experiment and theory agree we conclude that water molecules, and not sodium chloride ions, permeate through PDMS.

3.2.4 PEG Permeation through PDMS

We tested the molecular weight dependence of PEG permeability by creating salt free drops containing 18 %(w/v), 24 %(w/v) and 24 %(w/v) of PEG of 400, 1,000 and 8,000 molecular weight respectively. We performed similar experiments to those shown in Figure 3.3 in which we docked drops in wells containing salt-free PEG solutions and

reversibly varied the reservoir ionic strength to cycle the volume of the stored drop by a factor of two.

The assumption was that if over a five day period of several cycles the drops returned to their initial volume when the reservoir conditions were the same as initially then this would prove that the PEG remained in the drop and did not permeate through the PDMS membrane into the reservoir. If PEG left the drop, then the drop would contain only pure water and consequently would not be able to equilibrate against a reservoir containing a finite salt concentration. Because of the large molecular weight of PEG compared to NaCl the chemical potential difference between PEG solutions and pure water is much less than the chemical potential difference between salt solutions and pure water. For example, a 20 %(w/w) solution of PEG 8,000 has an osmotic pressure that is equivalent to a 0.15 M solution of NaCl. Extensive tables of the osmotic pressure of PEG solutions are available online (http://www.brocku.ca/researchers/peter_rand/osmotic/osfile.html).

Because of the small chemical potential difference between PEG solutions and pure water, the flux of water between the reservoir and docked PEG containing drops was small and comparable to the leakage flux to the exterior of the device, which led to noisy data. However, the conclusion (within 10 % experimental resolution) was that PEG does not permeate through PDMS. Surprisingly, this was true for all molecular weights, even for the 400 molecular weight PEG solutions.

3.3 Control of the Phase Behavior of PEG/Salt Mixtures

To demonstrate the performance of the Phase Chip, the phase diagram of a mixture of polymer and salt is measured. For certain compositions, mixtures of poly(ethylene) glycol (PEG) and ammonium sulfate in water will phase separate into two liquid phases, with one phase polymer-rich, the other phase salt-rich [78].

3.3.1 Preparation of Initial Condition

Figure 3.4 illustrates the procedure by which we initially prepare the samples and measure the salt and PEG concentrations on the Phase Chip.

First the Phase Chip generates a series of drops containing mixtures of PEG (molecular weight 3.35k, Sigma-Aldrich) and salt (Ammonium Sulfate, Sigma-Aldrich) whose concentrations vary in a linear fashion. We employ a technique developed for protein crystallization [31]. In this method there are two co-flowing aqueous streams, one of PEG and one of salt, which merge with two opposing oil streams at a nozzle, creating drops of the aqueous solution in the continuous oil phase.

The flow rates of the PEG and salt are periodically varied, with one increasing and one decreasing such that the total flow rate remains constant. Thus when drops are formed at the nozzle each drop has a different ratio of salt to PEG, but the volume of each drop is constant. Figure 3.4a demonstrates how drops whose ratio of PEG to salt varies linearly with time are created. The time scale of the experiment is 45 seconds. Each drop has a volume of 0.6 nl and a total of 250 wells were filled.

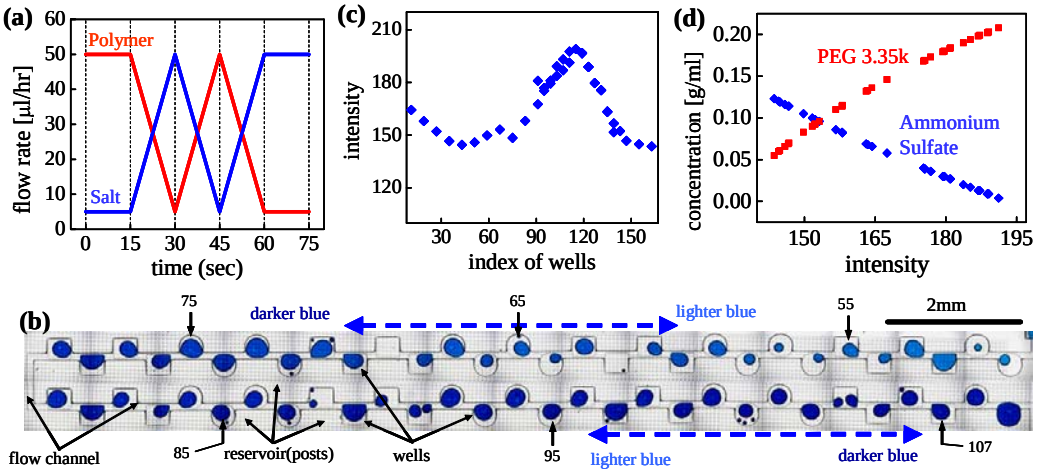

Figure 3.4 (a) Drop formulation. Flow rate profiles of polymer (PEG 3.35k) and salt (Ammonium sulfate) of co-flowing aqueous streams being fed into the drop generating nozzle. The polymer and salt concentrations of the stock solutions is 0.21 g/ml and 0.14 g/ml, respectively. **(b)** Drop storage. A portion of the Phase Chip shows blue dyed drops of the polymer/salt mixture solution stored in the wells. The concentration of ammonium sulfate is determined by measuring the light intensity passing through the each stored drop and the concentration of polymer is calculated from the salt concentration because the relative volumetric compositions of each drop are known from Figure 4a. **(c)** Light transmittance of the stored drops. The plot shows the light intensity transmitted through each drop in arbitrary units. The brighter drops have less of blue dye, which is proportional to the concentration of ammonium sulfate. **(d)** The initial concentrations of polymer and salt vs. light transmittances of each drop. The blue diamond represents ammonium sulfate, the red square is PEG 3.35k.

In Figure 3.4b a sequence of 60 wells filled with drops are shown. These wells are only slightly deeper than the channels so the surface tension forces holding the drops in place are weak (the slow-fast drop method in Chapter 2.4.2). When the flow rate is high the

drops flow pass the wells, but when the flow is suddenly cut using on-chip valves, surface tension forces lead the drops to dock into the nearest available well.

In order to measure the salt concentration in each drop 5 %(w/v) of a blue food dye (McCormic Corp.) is added into the ammonium sulfate stock solution. As shown in Figure 3.4b the color of each drop gradually changes from light blue (upper-right) to dark blue (lower-right) along the flow channel. The intensity of each drop indicates the concentration of ammonium sulfate; the darker the drop the higher the salt concentration and the intensity of transmitted light was measured using a video camera and digitizer.

The intensity varies smoothly with the index of drops as shown in Figure 3.4c demonstrating that drop formulation and storage was working as designed. The salt concentration is calculated from the intensity using a calibration table determined by filling the exact same microfluidic device with drops that all have the same known concentration of dye. The polymer concentration of each drop is calculated from the salt concentration since there is a specific volumetric relation between the ingredients as given by Figure 3.4a.

The volume fractions of salt and polymer in aqueous drops should be taken into account when the initial concentrations are estimated, because the drops are formulated with the volumetric ratio but the concentrations are calculated in weights of solutes and volume of solutions. Figure 3.4d shows the initial PEG and ammonium sulfate concentrations of the stored drops as a function of intensities, which are indexes of wells. Although some coalescence and breakage of drops occurs when manipulating the drops in the flow channel before they are docked into their storage wells, Figure 3.4c demonstrates that this mixing of drops does not involve enough drops to homogenize the composition gradient.

3.3.2 Driving the Phase Behavior of Drops

After preparing the initial conditions by formulating and storing drops and determining their composition by analyzing the intensity of the blue dye, the next step is to induce the liquid-liquid phase transition and to determine the PEG/salt composition at the phase boundary.

We drive the phase transition by removing water from the drops. This is accomplished by filling the reservoir with a 6 M NaCl solution. Initially, the salt concentration inside each of the drops is much less than 6 M so water flows out of the drops into the reservoir. As we concluded in Chapter 3.2.3 and 3.2.4 the drops retain all the salt and PEG placed there initially, which means the ratio of salt to PEG remains constant. However, the solute concentrations increase as water leaves the drops and the drops shrink in volume. Because only water permeates through the PDMS and because the height of the docked disk-shaped drops remains constant we can determine each solute concentration by measuring the area of the drop as a function of time: $X^{\mathrm{i}}_{\mathrm{drop}}(t) = X^{\mathrm{i}}_{\mathrm{o}} \cdot A_{\mathrm{o}} / A(t)$, with A_{o} and $A(t)$ the initial and time dependent area of the drop, respectively, and with $X^{\mathrm{i}}_{\mathrm{drop}}(t)$ and $X^{\mathrm{i}}_{\mathrm{o}}$ the time dependent and initial concentration of the solutes (PEG, ammonium sulfate), respectively. This method of determining concentration is more accurate than measuring the transmitted light intensity due to the presence of the blue dye.

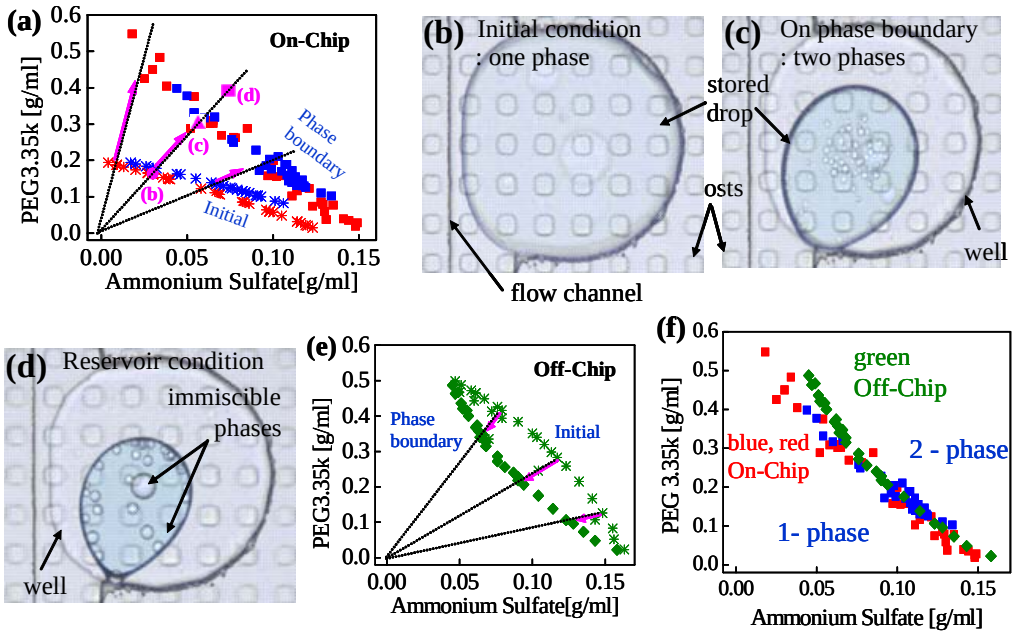

Figure 3.5 (a) The phase diagram of a mixture of PEG 3.35k and ammonium sulfate measured on the Phase Chip. The asterisks represent the initial conditions of drops stored on-chip. Different colors correspond to different trials. Square denote the phase boundary. The mixture is single liquid phase below the boundary and two liquid phases co-exist above the boundary. Water, but not salt or PEG is removed from the drops so the solute concentrations evolve along lines emanating from the origin. **(b),(c),(d).** The photographs show the appearance of the drops while the water is leaving the drop. The initially homogeneous solution (3.5b), which corresponds to the pink circle in (3.5a) denoted by the letter (b), separates into two phases shown in (3.5c), corresponding to the point on the phase boundary indicated by point (c) in (3.5a). In (3.5d) the drop has moved deeper into the two-phase region at the end of the experiment when the drop is in equilibrium with the reservoir. **(e)** The plot shows the phase diagram of the mixture measured off the Phase Chip with. The initial solutions (green asterisks) are prepared in the vial with concentrations above the phase boundary so they are in the two-phase state and have a cloudy appearance. Then water is added to the solution until it becomes clear, which signals a single, homogenous phase. The final concentration is calculated from the initial condition and the amount of water added onto the solution. **(f)** The two phase diagrams measured on- and off-chip are plotted together. The blue and red squares represent the on-chip measurements, the green diamond represents the off-chip data.

As the Phase Chip contains 250 wells and we are interested in determining the area of each drop (and hence its solute concentrations) as a function of time, an automated data acquisition and processing are desired. Automated imaging of each of the drops was performed using a robotic system designed for protein crystallization, the Rock Imager (Formulatrix, Waltham, MA). This system consists of a stepping motor driven XY translation stage and a color digital camera. The Rock Imager can be programmed to acquire images as a function of time and location and stores the images in a data base. After acquisition we process the images using an image recognition software package to measure the area of each drop (LabView, National Instruments).

After the reservoir is filled with 6 M salt solution the drops are allowed to shrink and equilibrate. During the entire process images are automatically and periodically acquired and the area of the drops is determined. After the initial concentration of the drops is determined by analyzing the intensity of transmitted light, the concentration of each of the solutes in the drop is subsequently calculated by measuring the area of the drop. The images of the drops are viewed and the point at which liquid-liquid phase separation is observed is noted as the phase boundary. Figure 3.5 illustrates this process.

In Figure 3.5b an image of a drop at the beginning of the experiment is shown. This drop has a composition indicated by point (b) in the phase diagram of Figure 3.5a. As the drop shrinks the concentrations of each solute in the drop increase, but because none of the solutes leave the drop the ratio of solute concentrations remain constant. This constrains the concentrations of a drop to linearly increase and the concentrations evolve along a line emanating from the origin. In Figure 3.5c the appearance of two liquid phases is first observed. By measuring the area of this drop the concentration of the solutes is determined and noted as point (c) in Figure 3.5a. The drop continues to shrink

until it equilibrates with the reservoir and this final state is shown in Figure 3.5d and its composition is marked as point (d) in Figure 3.5a. This process is repeated for each initial composition shown in Figure 3.5a in order to determine a complete phase diagram. The entire experiment was repeated with the same results, which demonstrates reproducibility, as illustrated in Figure 3.5a.

3.3.3 Phase Diagram Off-Chip

We validated the phase diagram obtained with the Phase Chip by measuring the phase diagram off-chip. Here we prepared a series of samples in the two phase region and then diluted the sample until the system became a single phase. We performed a dilution experiment because it is easier to add a solvent than to remove it when off-chip. Similarly to the on-chip case, the ratio of concentrations of the solutes remains constant as water is added to the mixture and the initial solute concentrations evolve along lines emanating from the origin.

The phase diagram obtained off-chip is shown in Figure 3.5e and the on-chip and off-chip phase diagrams are compared in Figure 3.5f. The on- and off-chip phase diagrams match except for low salt concentration. Measurement of the initial concentration of ammonium sulfate is inaccurate in this region because the blue dye is very dilute and is at the limits of sensitivity of our 8-bit digital camera. The off-chip measurements consumed 30 ml of solution in contrast to the on-chip measurements which consumed 50 μl.

3.3.4 Conclusions

We have manufactured a class of microfluidic devices designed to measure the phase diagrams of multi-component aqueous systems. The device consists of a formulation stage where the solute concentrations are varied, a droplet creation stage, and a droplet storage stage. The storage compartment contains a semi-permeable membrane through which water passes, but not protein, PEG, or salt. By constructing a reservoir on the other side of the membrane and filling the reservoir with a salt solution of a specific molarity, it is possible to controllably vary the water content of the drop.

The water permeability of the Phase Chip was experimentally investigated and quantitatively modeled with transport theory. Because the PDMS membranes are thin and the protein drops are small, the diffusion times are short and permeation is rapid. We built Phase Chips that were able to store 1 nl drops in wells at a density of $200/cm^2$ with an independent dialysis reservoir for each 20 wells. As a test of the Phase Chip the phase diagrams of PEG/ammonium sulfate solution were measured on-chip and validated off-chip.

The Phase Chip technology can be applied to other systems, such as the high throughput screening of conditions for protein crystallization. Because protein crystallization is a non-equilibrium process requiring one set of conditions for crystal nucleation and another set for crystal growth it makes sense to use the Phase Chip which allows dynamic control over the key thermodynamic variable; concentration as shown in Chapter 4. The Phase Chip, with its ability to reversibly control the water content of drops stored in wells, renders varying concentration as convenient as varying temperature.

Chapter 4

Protein Crystallization in the Phase Chip

4.1 Overview

In order to reveal the three-dimensional molecular structures of proteins, it is necessary to analyze protein crystals by x-ray diffraction [39]. Protein crystals are currently produced by trial and error, which requires exploring a large number of conditions and which consumes milligrams of protein. Non-microfluidic methods require about 1ml of solution per trial [39], while microfluidic devices reduce the volume per trial to 1nl or less [10, 49].

Reducing protein consumption, although important, is not the most pressing problem facing crystallographers. Rather, it is that crystallization is generally an activated process. Due to the surface tension between crystal and fluid there is an energy barrier that prevents the growth of crystals above a certain size [79].

As illustrated in Figure 4.1a the free energy (ΔG) of a spherical crystal nucleus of radius r in a protein solution is $\Delta G = \gamma 4\pi r^2 - \Delta\mu \, 4/3 \, \pi r^3$ with γ being the surface tension and $\Delta\mu$ the chemical potential difference of protein in the crystal and in the solution. The height of nucleation barrier (ΔG^*) and the critical nucleus radius (r^*) decrease as the

chemical potential difference ($\Delta\mu$) increase. This barrier is often quite large for proteins [80], so to achieve a finite nucleation rate, protein solutions in crystallization conditions should be highly supersaturated. Since the nucleation probability (Γ) is given by the negative exponential function of the energy barrier, according to the Boltzman's distribution law [81], a solution of higher concentration (large $\Delta\mu$) will have a higher nucleation probability, $\Gamma \propto \exp\left(-\Delta G^{*}/kt\right) = \exp\left(-16\pi\gamma^{3}/3kT\Delta\mu^{2}\right)$, and crystals, once nucleated, will grow rapidly if the radius is bigger than the critical nucleus radius (r*) [79]. However, under these conditions both the nucleation and growth rate are high, leading to the formation of many small defect-laden crystals that are unsuitable for x-ray diffraction.

The conundrum facing the crystallographer is that, while the nucleation of crystals requires deep supersaturation, the converse is true to grow large, defect-free crystals. Free interface diffusion, microbatch, and vapor diffusion are popular crystallization methods, which partially decouple the physical mechanisms of nucleation and growth [82, 83]. While these methods have been successfully implemented in microfluidics [5, 49, 84], their drawback is that they rely on irreversible kinetic processes, which are difficult to control and optimize.

This chapter explains a microfluidic implementation of dialysis and seeding. Our strategy for protein crystallization is to first formulate a combinatorial sequence of protein solutions of different salt and protein concentrations [31] as employed in Chapter 3.3.1 and subsequently store these drops in wells. Next these protein drops are concentrated by introducing air or a solution high in salt into the reservoir. Such conditions often lead to the creation of a large number of small crystals or small drops of

protein gel. We regard this material as seeds and subsequently change reservoir conditions by introducing pure water or solution low in salt into the reservoir. Water permeates from the reservoir into the protein solution and reduces the protein and salt concentrations, which lowers the chemical potential difference ($\Delta\mu$) between the protein in the solution and that in the crystal. This shifts the nucleation barrier causing the smaller nuclei to dissolve and the larger crystals to grow, thereby transforming the many small defective crystals into a few, large high quality crystals [79].

4.2 The Path on a Phase Diagram

The key technology exploited in the Phase Chip for realizing the decoupling is the reversible dialysis through PDMS membrane, whose fundamental concept is illustrated in the generic phase diagram in Figure 4.1b. The solid black lines represent the liquid–crystal phase boundary. Dashed tie-lines connect co-existing concentrations, with crystals high in protein and low in precipitants such as PEG.

Step 1: The initial concentration is a stable solution (red circles - points a).

Step 2: Dialysis against a solution high in salt removes water from the drop, concentrating the protein and precipitant (path $a \rightarrow b$), which increases the chemical potential difference ($\Delta\mu_3 \rightarrow \Delta\mu_1$) hence lowering the free energy barrier ($\Delta G_3^* \rightarrow \Delta G_1^*$) and the critical radius (r^*). At point b, the solution is metastable and if crystals nucleate then phase separation occurs along tie-lines (path $b \rightarrow b'$) producing many small crystals that grow rapidly.

Step 3: Dialysis against a solution low in salt adds water to the drop, diluting the protein and precipitant, which lowers $\Delta\mu$ and increases ΔG^* and r^*, suppressing further

nucleation, causes the small crystals to melt along the equilibrium phase boundary (path $b' \rightarrow c'$), and slows the growth into large crystals. If there was no nucleation or phase separations at point b then the metastable solution would evolve along the path $b \rightarrow c$.

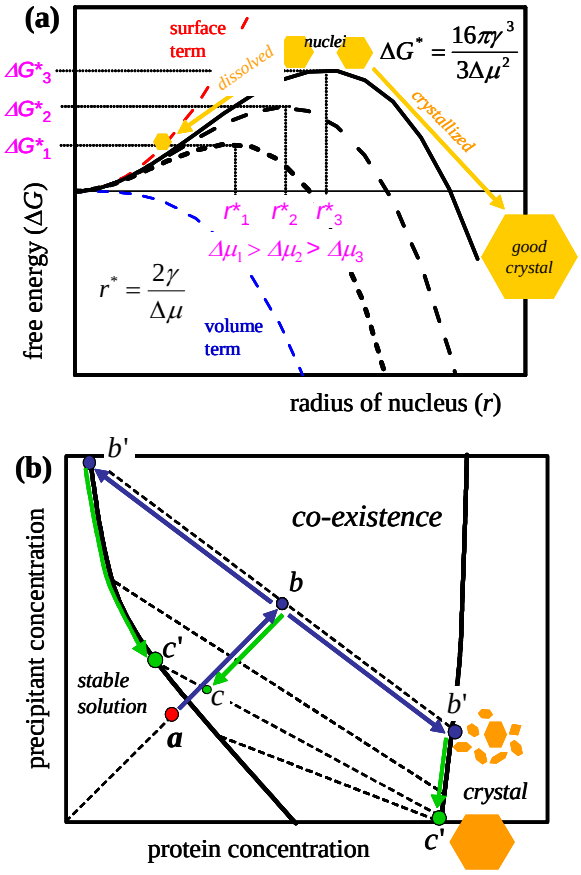

Figure 1. (a) The energy barrier (ΔG^*) and the critical radius (r^*) of the nucleus are determined by the chemical potential ($\Delta\mu$). **(b)** The generic phase diagram. At point *b*, the drop is the highly supersaturated region where the chemical potential is $\Delta\mu_1$ in (a) and the barrier height is at its lowest (ΔG_1^*), many nuclei are born (point b'): nucleation. While diluting the drop ($\Delta\mu_1 \rightarrow \Delta\mu_2 \rightarrow \Delta\mu_3$), the energy barrier gets higher ($\Delta G_1^* \rightarrow \Delta G_2^* \rightarrow \Delta G_3^*$), then the nuclei being bigger than r_3^* can grow into good crystals, hence, crystal growth occurs. Otherwise, the nuclei dissolve.

4.3 Experiments and Results

4.3.1 Crystallization and Melting

In order to demonstrate the capability of the Phase Chip to utilize the reversible dialysis for protein crystallization, we crystallized one of the prototype proteins, xylanase. Xylanase has a molecular weight of 21kD and consists of 190 amino acids [85]. The protein is a class of enzymes that breaks down hemicellulose, which is a major component of the cell wall of plants [86]. Its optimum activity is around pH 5.3, and the isoelectric point is pH 9.0. Xylanase can be crystallized at a protein concentration of 2 mg/ml to 17 mg/ml by the hanging drop method in a potassium phosphate buffer between pH 7 and pH 8.2, or ammonium sulfate buffer at pH 4.3 (Hampton Research).

A stock solution of xylanase is obtained from Hampton research at 36 mg/ml concentration. Although the stock solution contains 43 %(w/v) of glycerol and 0.18 M of Na/K phosphate at pH 7, no further dialysis is done. The protein solution is prepared by adding sodium chloride solution into the stock solution leading to final salt and protein concentrations of 0.5 M and 4.5 mg/ml respectively.

In the crystallization experiment, the solution is injected into the Phase Chip and stored in the wells. In order to obtain statistics on the crystallization process, all drops contain the same protein and buffer. Because the drops are identical there is no need to stabilize them against coalescence. For this experiment the oil is a mixture of PFD (Perfluorodecaline, Sigma-Aldrich) and 12%(w/w) Tridecafluoro-1-octanol (Sigma-Aldrich). Although the drops do not form stable emulsions in this oil with the surfactant; instead, they merge then break apart as they pass over occupied wells, the surface

tensional force is increased enough to be able to generate protein drops in the moving phase.

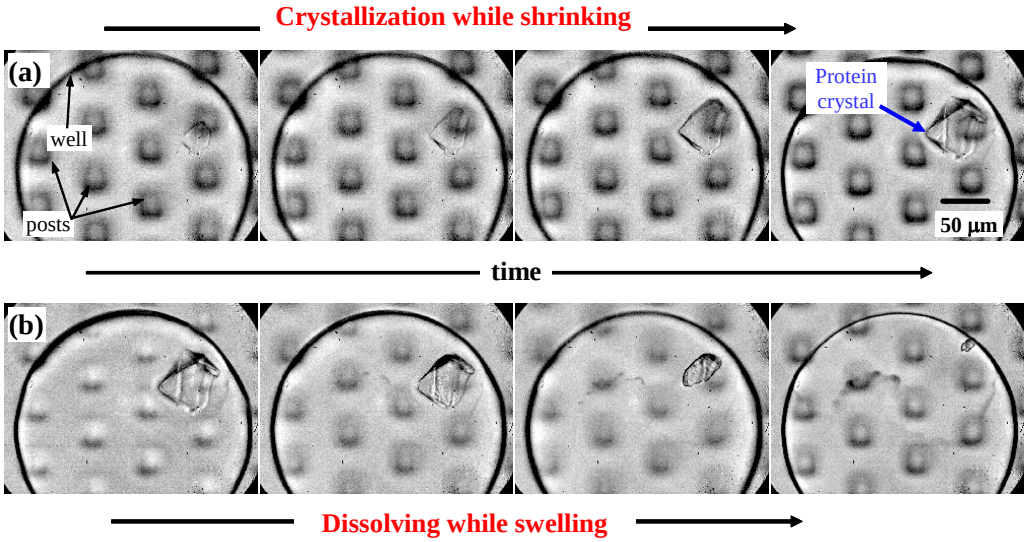

Figure 4.2 Photographs of Spontaneous crystallization and Dissolving of Xylanase. The round circle is the well and the square posts are the membrane supports that are fabricated in the reservoir. There is a PDMS membrane between these two layers, which is 15 µm. **(a)** Crystallization occurs when dry air is circulated in the reservoir driving the water molecules which are transported from the protein solution through the membrane and into the reservoir. **(b)** The crystal dissolves when the pure water flows in the reservoir so that the water molecules are transported from the reservoir into the drop containing the protein crystals. After melting the crystal completely, if water is removed from the drop again, crystallization occurs. The crystals have different shapes and come out at random location in the same well.

Xylanase is soluble under these conditions and drops containing protein are stored in about 100 wells. Air is then introduced into the reservoir to build the chemical potential and the drops are observed to shrink. After 15 minutes crystals begin to form and by 20 minutes approximately 80 % of the wells have crystals, which grow to their maximal size

in one minute. Some wells have a single crystal while other wells have multiple crystals. After 30 minutes the air in the reservoir is replaced with water and the solution surrounding the crystals begin to grow. After 30 minutes the crystals begin to melt rapidly, and they vanish in another minute. The cycle of crystallization and melting occurs repeatedly a few times in a very controlled way by changing the reservoir conditions. Figure 4.2 shows the crystallization and melting of xylanase in a prototype Phase Chip.

This experiment shows the feasibility of crystallizing proteins using sub-nanoliter volumes in microfluidic devices practicing the reversible dialysis. The crystallization in Figure 4.2 is not initiated with decoupling nucleation and crystal growth. The protein stored in the wells at deep supersaturation after the shrinkage is spontaneously crystallized. The following chapter will show the experiment employing the decoupling strategy in which crystallization is more likely than with spontaneous nucleation.

4.3.2 Crystallization with the Decoupling

In this chapter, the discussion will focus on the usefulness of the decoupling strategy for protein crystallization, implemented in the microfluidic system exploiting the reversible dialysis. For this experiment, the protein solution of xylanase is used as in the previous chapter, but, the solution is prepared in a different way. The stock solution of protein (Hampton Research, HR7-104) is dialyzed against 0.4 M potassium sodium tartrate tetrahydrate (Crystal Screen HR2-110, Hampton Research) and the initial protein concentration is 15.3 mg/ml. Xylanase does not crystallize under these conditions. When the protein solution is injected and docked into the wells, the mixture of PFD

(perfluorodecailne) and 12 %(w/w) of Tridecafluoro-1-octanol is used as a continuous phase. All the drops stored in the wells are identical as well.

A 5 M NaCl solution is introduced into the reservoir, causing water to be permeated out of the protein solution. After 2.5 hours, the protein solution in the drop is concentrated to approximately 20 mg/ml, at which point the protein solution becomes unstable and forms numerous drops of a dense protein gel as shown in Figure 4.3c. The gel is a non-equilibrium state often observed in highly supersaturated protein solutions [87]. Next, the reservoir solution is changed to pure water, which causes water to flow from the reservoir to the protein solution and lowers the degree of supersaturation. Under these conditions nucleation theory predicts that large crystals grow at the expense of small ones, as illustrated in Figure 4.1 [79]. A photograph, taken six days later, shows that the protein gel transformed into needle-shaped crystals (Figure 4.3d).

This is evidence that the Phase Chip stimulates the nucleation of protein when the dialysis through the PDMS membrane drives the protein solution into the region of high supersaturation, as explained in Figure 4.1b. Furthermore, the Phase Chip induces growth of protein crystals when this reversible dialysis brings the nuclei, which are born while the drop shrinks, into the region of lower supersaturation. We have observed same scenario with another protein, lysozyme, albeit in a more systematic way.

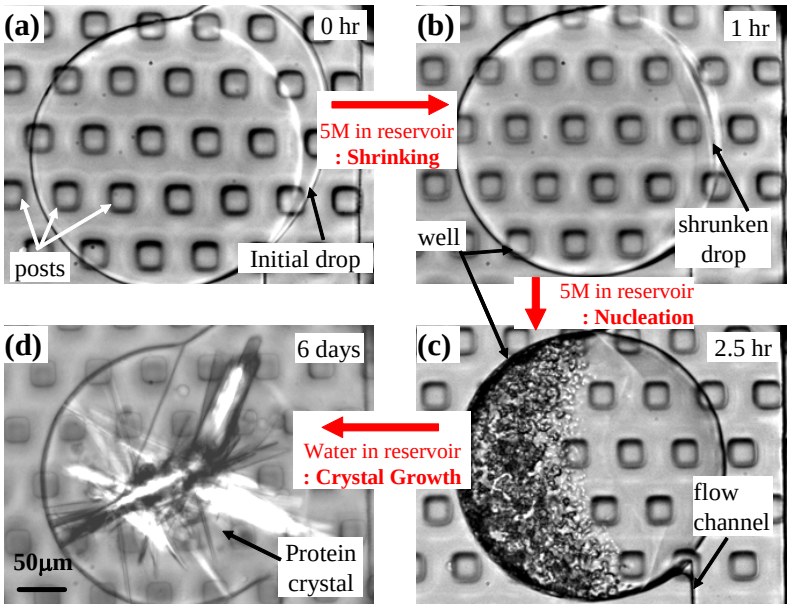

Figure 4.3 Protein crystallization with the decoupling nucleation and crystal growth. The series of photographs shows a 300 μm diameter circular well that contains the protein of xylanase dissolved in potassium sodium tartrate tetrahydrate solution. The flow channel is on the right side of the well. The square posts are 30 μm wide and support a 15μm PDMS membrane, which forms the bottom of the well. **(a)** A stable protein solution of xylanase slightly overfills the well. **(b)** The drop shrinks as 5 M NaCl solution flows in reservoir. **(c)** Protein gelation occurs. The nuclei, which will grow into the crystal at later stage, are born in the gel either (nucleation). **(d)** The reservoir is filled with pure water, which hydrated the precipitate, transforming nuclei into crystals (crystal growth).

4.3.3 Systematic Experiment using Decoupling Methodology

The experiment described in the previous chapter shows the feasibility of protein crystallization using the decoupling strategy in the microfluidic system which employs the reversible dialysis. In order to clarify the applicability of the strategy accommodated

in the microfluidic device, a systematic experiment is required to show statistical differences of crystallization probabilities with or without the strategy.

For performing systematic experiments, the new version of a microfluidic device is designed. This type of device is shown in detail in Figure 2.1. The Phase Chip has four storage areas and five independent reservoirs, so salt solutions of five different molarities can be applied to each storage area. First, a single-condition protein solution is stored in wells, then at least two different chemical potentials are applied to the storage. Since conditions of each reservoir are individually controllable, a partial region of the storage is always set by a condition, while another partial region has different conditions as a function of time, as illustrated in Figure 4.4.

For this experiment, lysozyme is used. The egg white lysozyme is a polypeptide of 129 amino acid residues with a molecular weight of 14.4kD. It is a positively charged protein with an isoelectric point of 10.7 ~ 11.0 [88]. Lysozyme is an enzyme commonly referred to as the body's own antibiotic since it kills bacteria.

Lysozyme that has been crystallized six times is obtained from Seikagaku America (Falmouth, MA). The protein is used without further purification. All the chemicals used in preparing solutions are purchased from Sigma-Aldrich. A Millipore (Billerica, MA) Elix system produces purified water for use as a solvent. A mixture of 19.5 mg/ml lysozyme and 10 %(w/w) Poly(ethylene) glycol (PEG) is dissolved in 0.2 M NaAc-trihydrate, 0.1 M NaCacodylate at pH 6.5. The molecular weight of PEG is 8000 g/mol. The pH is measured by a pH meter (Orion SA520). When drops of the protein solution are stored in the wells, a fluorinated oil (FC-43, 3M) mixed with 15 %(w/w) of Tridecafluoro-1-octanol is employed as a moving phase. All the drops stored in the wells are identical.

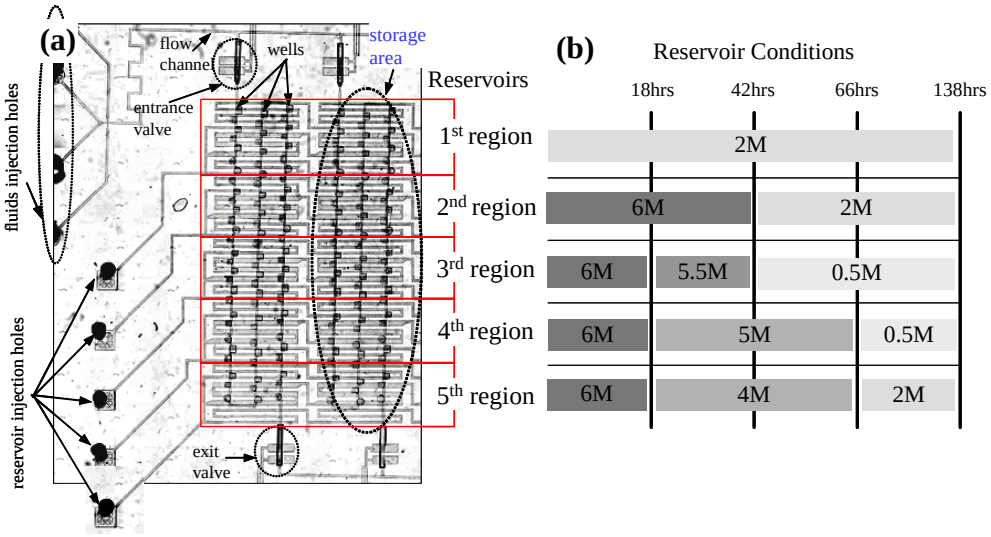

Figure 4.4. (a) A photograph showing a part of the device used for the experiment. This version is the latest design. It has five independently controllable reservoirs for each storage area. All storage wells have an identical drop condition. **(b)** The chart shows reservoir conditions as a function of time. The 1st area always stays on the 2 M NaCl solution, circulating in the reservoir. The rest of reservoir has 6 M in the beginning. In order to find the appropriate shallow supersaturation, where slow crystal growths occur while further nucleation is suppressed, a number of lower molar NaCl solutions are applied into the reservoir: 5.5 M, 5 M, 4 M, 2 M and 0.5 M.

After storing drops in the wells, 2 M and 6 M of NaCl solutions are introduced into the first and the rest of reservoirs respectively. Each reservoir condition gives different chemical potentials to the protein drops that are sitting above the corresponding reservoir. The reservoir having 6 M NaCl solution leads the protein drops into a deep supersaturation region in the phase diagram shown in Figure 4.1 than the reservoir having 2 M NaCl solution does. Figure 4.4b shows the temporal sequence of reservoir conditions in order to investigate how the decoupling strategy works for protein crystallization. Afterwards, the reservoir with the 6 M solution is switched with lower molar NaCl

solutions that drive the protein drops, which used to be in the deep supersaturation region, into a region of shallow supersaturation where crystal growth continues while nucleation is depressed. Photographs of all regions of the device are taken with an automated benchtop imaging system, the Rock Imager, which was donated by Formulatrix.

As shown in Figure 4.5, protein crystals grow in the wells in various ways. In the 1st storage region, only one out of five wells has a protein crystal, while all six wells have crystals in the 2nd storage region. The initial and the final conditions of both reservoirs are the same. The difference is a kinematical path in the phase diagram.

The 1st storage region stays on the 2 M reservoir for 138 hours, where the drops are always clear and only one crystal comes out. The 2nd storage region firstly stays in deep supersaturation (6 M) for 42 hours, where the protein solutions are unstable and the precipitation happens (the black aggregations in the drops). When the drops having precipitations are exposed to the less salty reservoir (2 M), water transports from the reservoir to the protein drops. Then the aggregation dissolves and the drops become clear. 24 hours after replacing the reservoir condition with 2 M, three wells are crystallized. Furthermore, within an additional 72 hours, three more wells in the 2nd storage region have protein crystals.

We claim that during the precipitation process many nuclei are born in the protein drop, and, if the protein drop is brought into the region of the shallow supersaturation (2 M), the nuclei, which overcome the free energy barrier $\left(\Delta G^* = \frac{16\pi\gamma^3}{3\Delta\mu^2} \right)$, grow into crystals. This is a clear evidence of the decoupling strategy, realized in the microfluidic device, being able to accelerate protein crystallization.

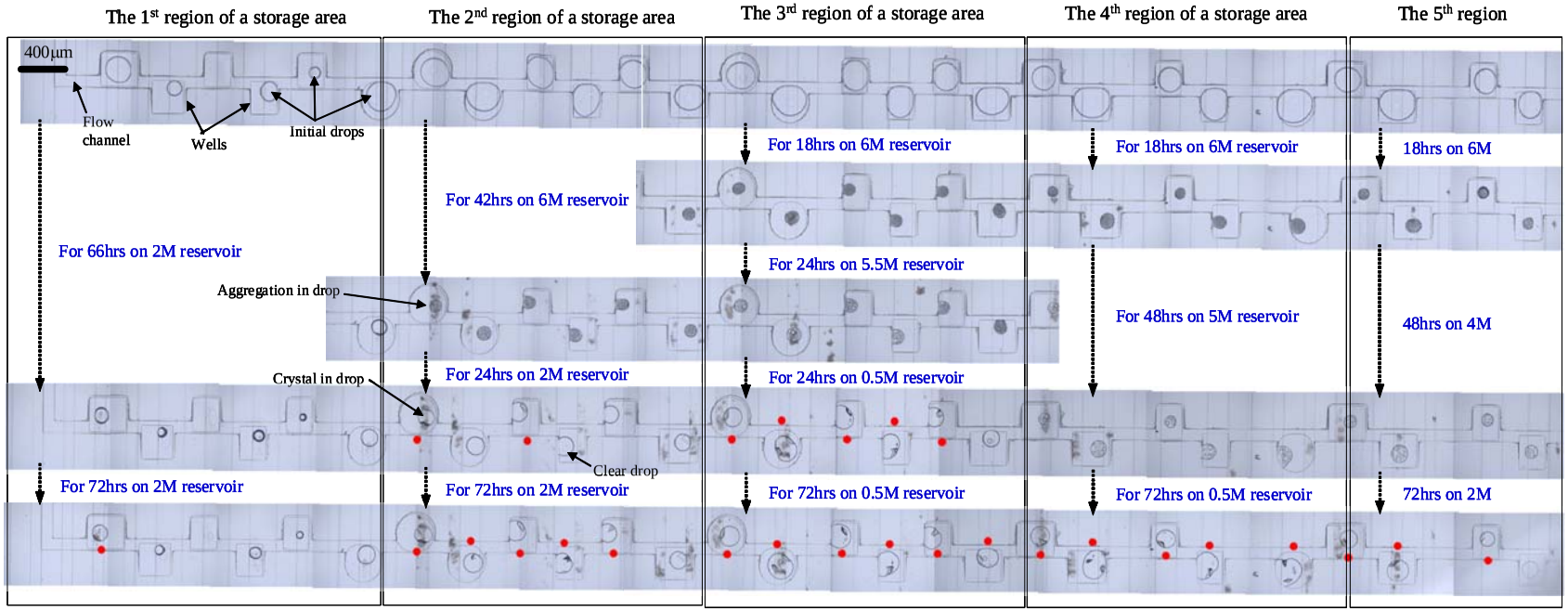

Figure 4.5. The stitched photographs are showing a part of flow channel in a storage area. Each photograph, running horizontally, is taken as a function of time; initial, 18 hour, 42 hour, 66 hour and 138 hour. Each black box represents a region of the storage area, which has its independently controllable reservoir condition. The red dots indicate wells that have protein crystals. 2 M salt solution flows in reservoir of the 1st storage region, only one well out of five has a crystal within 138 hours. 6 M solution is circulated in the 2nd storage region, the protein drop aggregates first. The reservoir for the 2nd storage region is replaced with 2 M, the drop become clear and subsequently crystallizations occur.

A number of reservoir conditions are tested in order to find the most efficient shallow supersaturation region for optimizing crystal growth. Although the reservoir condition of the 3rd, 4th and 5th regions of the storage are replaced with 5.5 M, 5 M and 4 M salt solutions respectively, as shown in Figure 4.5, the aggregations still stay in the protein drops. However, the lower salt solutions (2 M, 0.5 M) can dissolve them, and enhances crystal growth. For the protein solution employed in this experiment, a range of 3 M to 6 M NaCl solution in reservoirs is a deep supersaturation region, named 'nucleation zone', and a range of 0.5M to 2M is a shallow supersaturation region, called 'metastable zone', as defined in Chayen et al [83].

4.3.4 Decoupling Off-Chip

In order to ascertain the crystallization behavior with respect to the kinematical paths, a protein crystallization experiment is done by the conventional vapor diffusion method: the hanging drop method. This experiment was performed with Dr. Yanwei Jia, a post doctoral researcher of Prof. Seth Fraden's group.

The condition of the protein solution is identical with the one used in the microfluidic device; 20 mg/ml lysozyme and 10 %(w/w) Poly(ethylene) glycol (PEG) dissolved in 0.2 M NaAc-trihydrate, 0.1 M NaCacodylate at pH 6.5. As illustrated in Figure 4.6a, the Libro plate, containing 1 ml of 6 M or 2 M NaCl solution, is covered with a glass slide (Cover glass, Gold Seal), on which 4 μl of the protein solution is pipetted. The glass slide is sealed on the Libro plates with a grease rim. They are stored in a place where there is no disturbance, which may cause spontaneous crystallization. One Libro plate has 2 M solution in the reservoir all the time. Another plate has 2 M solution in the beginning,

then the reservoir is replaced with 6 M solution three days later, which is similar to the reservoir-changing conditions in the Phase Chip.

Figure 4.6b shows a protein crystal spontaneously nucleated on the 2 M reservoir in Libro plate, while Figure 4.6c shows crystallization activated by decoupling in the Libro plate. 70 hours after the protein drop is exposed to the 6 M reservoir, the glass slides that had aggregated proteins are moved to another Libro plate, which has the 2 M NaCl solution in the reservoir. The protein drops become clear, and subsequently protein crystals grow. This result shows that the crystallization, which happens with the conventional vapor diffusion method, is able to be reproduced in the microfluidic device utilizing the reversible dialysis with a lot smaller amount of protein solutions.

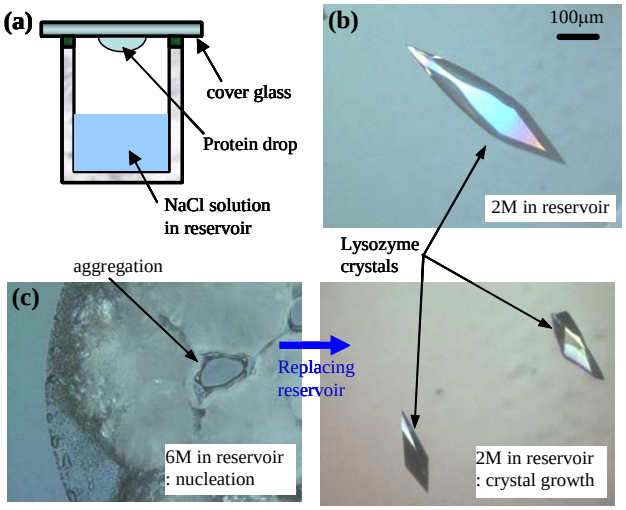

Figure 4.6 (a) A schematic diagram of the Libro plate used in the experiment employing the vapor diffusion method. The chemical potential between a drop and reservoir is driving the transportation of water vapors. **(b)** A protein crystal grown on 2 M reservoir. The photograph is taken under polarizer. **(c)** Protein crystals nucleated on 6 M reservoir (left) and crystallized in the 2 M reservoir (right). The circular artifact on the left is the boundary of the protein drop hung underneath the glass slide. These photographs are taken with the same magnification.

4.4 Concluding Remarks

Other than previously reported microfluidic implementations, the Phase Chip can decouple the physical processes of protein crystal nucleation and growth. The water contents of the stored drops are reversibly controlled with the incorporating a dialysis membrane that is permeable to water. The reversible controllability presents several advantages for protein crystallization.

First, protein crystallization is a non-equilibrium process so it makes sense to have dynamic control over the key thermodynamic variable; concentration. The Phase Chip, with its ability to reversibly control protein and precipitant concentrations, renders varying concentration as convenient as varying temperature. Second, by varying the water content of each drop we can explore many different crystallization conditions in the same drop. Finally, we have demonstrated that we can first formulate stable protein solutions, next induce nucleation and then grow large protein crystals. We speculate that the ability to reversibly grow and dissolve protein crystals can be exploited to salvage defective crystals and transform small crystals into large ones through repetitive crystallization cycles.

Because the PDMS membranes are thin and the protein drops are small, the diffusion times are short and the dialysis is quick. For these reasons, the Phase Chip promises to be a faster, better, and cheaper method for the protein crystallization.

Bibliography

1. McDonald, J.C., et al., *Fabrication of microfluidic systems in poly(dimethylsiloxane).* Electrophoresis, 2000. **21**(1): p. 27-40.

2. Lee, S., D.H. Kim, and D. Needham, *Equilibrium and dynamic interfacial tension measurements at microscopic interfaces using a micropipet technique. 1. A new method for determination of interfacial tension.* Langmuir, 2001. **17**(18): p. 5537-5543.

3. Studer, V., et al., *Scaling properties of a low-actuation pressure microfluidic valve.* Journal Of Applied Physics, 2004. **95**(1): p. 393-398.

4. Zheng, B., et al., *A droplet-based, composite PDMS/glass capillary microfluidic system for evaluating protein crystallization conditions by microbatch and vapor-diffusion methods with on-chip X-ray diffraction.* Angewandte Chemie-International Edition, 2004. **43**(19): p. 2508-2511.

5. Hansen, C.L., et al., *A robust and scalable microfluidic metering method that allows protein crystal growth by free interface diffusion.* Proceedings Of The National Academy Of Sciences Of The United States Of America, 2002. **99**(26): p. 16531-16536.

6. Beebe, D.J., G.A. Mensing, and G.M. Walker, *Physics and applications of microfluidics in biology.* Annual Review Of Biomedical Engineering, 2002. **4**: p. 261-286.

7. Luft, J.R. and G. DeTitta, *Kinetic aspects of macromolecular crystallization*, in *Macromolecular Crystallography, Pt A*. 1997. p. 110-131.

8. Hong, J.W. and S.R. Quake, *Integrated nanoliter systems.* Nature Biotechnology, 2003. **21**(10): p. 1179-1183.

9. Stone, H.A., A.D. Stroock, and A. Ajdari, *Engineering flows in small devices: Microfluidics toward a lab-on-a-chip.* Annual Review Of Fluid Mechanics, 2004. **36**: p. 381-411.

10. Squires, T.M. and S.R. Quake, *Microfluidics: Fluid physics at the nanoliter scale.* Reviews Of Modern Physics, 2005. **77**(3): p. 977-1026.

11. Dittrich, P.S., K. Tachikawa, and A. Manz, *Micro total analysis systems. Latest advancements and trends.* Analytical Chemistry, 2006. **78**(12): p. 3887-3907.

12. Whitesides, G.M., *The origins and the future of microfluidics.* Nature, 2006. **442**(7101): p. 368-373.

13. Liu, R.H., et al., *Passive mixing in a three-dimensional serpentine microchannel.* Journal Of Microelectromechanical Systems, 2000. **9**(2): p. 190-197.

14. Song, H., et al., *Experimental test of scaling of mixing by chaotic advection in droplets moving through microfluidic channels.* Applied Physics Letters, 2003. **83**(22): p. 4664-4666.

15. Niu, X.Z. and Y.K. Lee, *Efficient spatial-temporal chaotic mixing in microchannels.* Journal Of Micromechanics And Microengineering, 2003. **13**(3): p. 454-462.

16. Groisman, A. and S.R. Quake, *A microfluidic rectifier: Anisotropic flow resistance at low Reynolds numbers.* Physical Review Letters, 2004. **92**(9).

17. Stroock, A.D., et al., *Chaotic mixer for microchannels.* Science, 2002. **295**(5555): p. 647-651.

18. Thorsen, T., et al., *Dynamic pattern formation in a vesicle-generating microfluidic device.* Physical Review Letters, 2001. **86**(18): p. 4163-4166.

19. Anna, S.L., N. Bontoux, and H.A. Stone, *Formation of dispersions using "flow focusing" in microchannels.* Applied Physics Letters, 2003. **82**(3): p. 364-366.

20. Tice, J.D., et al., *Formation of droplets and mixing in multiphase microfluidics at low values of the Reynolds and the capillary numbers.* Langmuir, 2003. **19**(22): p. 9127-9133.

21. Stone, H.A., *Dynamics Of Drop Deformation And Breakup In Viscous Fluids.* Annual Review Of Fluid Mechanics, 1994. **26**: p. 65-102.

22. Dreyfus, R., P. Tabeling, and H. Willaime, *Ordered and disordered patterns in two-phase flows in microchannels.* Physical Review Letters, 2003. **90**(14).

23. Link, D.R., et al., *Geometrically mediated breakup of drops in microfluidic devices.* Physical Review Letters, 2004. **92**(5).

24. Tan, Y.C., et al., *Design of microfluidic channel geometries for the control of droplet volume, chemical concentration, and sorting.* Lab On A Chip, 2004. **4**(4): p. 292-298.

25. Link, D.R., et al., *Electric control of droplets in microfluidic devices.* Angewandte Chemie-International Edition, 2006. **45**(16): p. 2556-2560.

26. Chou, C.F., et al., *A miniaturized cyclic PCR device - modeling and experiments.* Microelectronic Engineering, 2002. **61-2**: p. 921-925.

27. Erickson, D., et al., *Electrokinetically based approach for single-nucleotide polymorphism discrimination using a microfluidic device.* Analytical Chemistry, 2005. **77**(13): p. 4000-4007.

28. Guber, A.E., et al., *Microfluidic lab-on-a-chip systems based on polymers - fabrication and application.* Chemical Engineering Journal, 2004. **101**(1-3): p. 447-453.

29. Sia, S.K., et al., *An integrated approach to a portable and low-cost immunoassay for resource-poor settings.* Angewandte Chemie-International Edition, 2004. **43**(4): p. 498-502.

30. Nam, K.H., et al., *Continuous-flow fractionation of animal cells in microfluidic device using aqueous two-phase extraction.* Biomedical Microdevices, 2005. **7**(3): p. 189-195.

31. Zheng, B., L.S. Roach, and R.F. Ismagilov, *Screening of protein crystallization conditions on a microfluidic chip using nanoliter-size droplets.* Journal Of The American Chemical Society, 2003. **125**(37): p. 11170-11171.

32. Choban, E.R., et al., *Microfluidic fuel cell based on laminar flow.* Journal Of Power Sources, 2004. **128**(1): p. 54-60.

33. Hayes, R.A. and B.J. Feenstra, *Video-speed electronic paper based on electrowetting.* Nature, 2003. **425**(6956): p. 383-385.

34. Chang, I.H., et al., *Miniaturized lead sensor based on lead-specific DNAzyme in a manocapillary interconnected microfluidic device.* Environmental Science & Technology, 2005. **39**(10): p. 3756-3761.

35. Piazza, R., *Interactions and phase transitions in protein solutions.* Current Opinion In Colloid & Interface Science, 2000. **5**(1-2): p. 38-43.

36. George, A. and W.W. Wilson, *Predicting Protein Crystallization from a Dilute-Solution Property.* Acta Crystallographica Section D-Biological Crystallography, 1994. **50**: p. 361-365.

37. Guo, B., et al., *Correlation of second virial coefficients and solubilities useful in protein crystal growth.* Journal Of Crystal Growth, 1999. **196**(2-4): p. 424-433.

38. McPherson, A., *Introduction - Macromolecular crystallization in the structural genomics era.* Journal Of Structural Biology, 2003. **142**(1): p. 1-2.

39. McPherson, A., *Crystallization of biological macromolecules*. 1999, Cold Spring Harbor, NY: Cold Spring Harbor Laboratory Press. 586.

40. Bergfors, T., *Seeds to crystals.* Journal Of Structural Biology, 2003. **142**(1): p. 66-76.

41. Chernov, A.A. and L.J. DeLucas, *View on biocrystallization from Jena, 2002.* Acta Crystallographica Section D-Biological Crystallography, 2002. **58**: p. 1511-1513.

42. Smith, H.W. and L.J. Delucas, *A Method For Programmable Control Of Reservoir Concentrations For Protein Crystal-Growth.* Journal Of Crystal Growth, 1991. **110**(1-2): p. 137-141.

43. Lee, S.S.J. and R. Cudney, *A modified microdialysis button for use in protein crystallization.* Journal of Applied Crystallography, 2004. **37**: p. 504-505.

44. Hansen, C. and S.R. Quake, *Microfluidics in structural biology: smaller, faster... better.* Current Opinion in Structural Biology, 2003. **13**(5): p. 538-544.

45. Song, H. and R.F. Ismagilov, *Millisecond kinetics on a microfluidic chip using nanoliters of reagents.* Journal of the American Chemical Society, 2003. **125**(47): p. 14613-14619.

46. Song, H., J.D. Tice, and R.F. Ismagilov, *A microfluidic system for controlling reaction networks in time.* Angewandte Chemie-International Edition, 2003. **42**(7): p. 768-772.

47. Yi, G.R., et al., *Generation of uniform colloidal assemblies in soft microfluidic devices.* Advanced Materials, 2003. **15**(15): p. 1300-+.

48. Sia, S.K. and G.M. Whitesides, *Microfluidic devices fabricated in poly(dimethylsiloxane) for biological studies.* Electrophoresis, 2003. **24**(21): p. 3563-3576.

49. Zheng, B., C.J. Gerdts, and R.F. Ismagilov, *Using nanoliter plugs in microfluidics to facilitate and understand protein crystallization.* Current Opinion In Structural Biology, 2005. **15**(5): p. 548-555.

50. Chen, D.L., C.J. Gerdts, and R.F. Ismagilov, *Using microfluidics to observe the effect of mixing on nucleation of protein crystals.* Journal Of The American Chemical Society, 2005. **127**(27): p. 9672-9673.

51. Lee, J.N., C. Park, and G.M. Whitesides, *Solvent compatibility of poly(dimethylsiloxane)-based microfluidic devices.* Analytical Chemistry, 2003. **75**(23): p. 6544-6554.

52. Favre, E., et al., *Sorption, Diffusion And Vapor Permeation Of Various Penetrants Through Dense Poly(Dimethylsiloxane) Membranes - A Transport Analysis.* Journal Of Membrane Science, 1994. **92**(2): p. 169-184.

53. Manz, A., et al., *Design Of An Open-Tubular Column Liquid Chromatograph Using Silicon Chip Technology.* Sensors And Actuators B-Chemical, 1990. **1**(1-6): p. 249-255.

54. Harrison, D.J., et al., *Micromachining A Miniaturized Capillary Electrophoresis-Based Chemical-Analysis System On A Chip.* Science, 1993. **261**(5123): p. 895-897.

55. Effenhauser, C.S., et al., *Integrated capillary electrophoresis on flexible silicone microdevices: Analysis of DNA restriction fragments and detection of single DNA molecules on microchips.* Analytical Chemistry, 1997. **69**(17): p. 3451-3457.

56. Srinivasan, V., V.K. Pamula, and R.B. Fair, *Droplet-based microfluidic lab-on-a-chip for glucose detection.* Analytica Chimica Acta, 2004. **507**(1): p. 145-150.

57. Zhu, L., C.S. Lee, and D.L. DeVoe, *Integrated microfluidic UV absorbance detector with attomol-level sensitivity for BSA.* Lab On A Chip, 2006. **6**(1): p. 115-120.

58. Weigl, B.H. and P. Yager, *Microfluidics - Microfluidic diffusion-based separation and detection.* Science, 1999. **283**(5400): p. 346-347.

59. Shaw, J.M., et al., *Negative photoresists for optical lithography.* Ibm Journal Of Research And Development, 1997. **41**(1-2): p. 81-94.

60. Duffy, D.C., et al., *Rapid prototyping of microfluidic systems in poly(dimethylsiloxane).* Analytical Chemistry, 1998. **70**(23): p. 4974-4984.

61. Unger, M.A., et al., *Monolithic microfabricated valves and pumps by multilayer soft lithography.* Science, 2000. **288**(5463): p. 113-116.

62. Whitesides, G.M., et al., *Soft lithography in biology and biochemistry.* Annual Review Of Biomedical Engineering, 2001. **3**: p. 335-373.

63. Blume, I., J.G. Wijmans, and R.W. Baker, *The Separation Of Dissolved Organics From Water By Pervaporation.* Journal Of Membrane Science, 1990. **49**(3): p. 253-286.

64. Ng, J.M.K., et al., *Components for integrated poly(dimethylsiloxane) microfluidic systems.* Electrophoresis, 2002. **23**(20): p. 3461-3473.

65. Crank, J., *The mathematics of diffusion*. 2nd ed. 1975, Oxford: Clarendon Press. 399.

66. Chayen, N.E., *Comparative studies of protein crystallization by vapour-diffusion and microbatch techniques.* Acta Crystallographica Section D-Biological Crystallography, 1998. **54**: p. 8-15.

67. Tamai, Y., H. Tanaka, and K. Nakanishi, *Molecular Simulation Of Permeation Of Small Penetrants Through Membranes .2. Solubilities.* Macromolecules, 1995. **28**(7): p. 2544-2554.

68. Tamai, Y., H. Tanaka, and K. Nakanishi, *Molecular Simulation Of Permeation Of Small Penetrants Through Membranes .1. Diffusion-Coefficients.* Macromolecules, 1994. **27**(16): p. 4498-4508.

69. Watson, J.M. and M.G. Baron, *Precise Static And Dynamic Permeation Measurements Using A Continuous-Flow Vacuum Cell.* Journal Of Membrane Science, 1995. **106**(3): p. 259-268.

70. Randall, G.C. and P.S. Doyle, *Permeation-driven flow in poly(dimethylsiloxane) microfluidic devices.* Proceedings Of The National Academy Of Sciences Of The United States Of America, 2005. **102**(31): p. 10813-10818.

71. Lotters, J.C., et al., *The mechanical properties of the rubber elastic polymer polydimethylsiloxane for sensor applications.* Journal Of Micromechanics And Microengineering, 1997. **7**(3): p. 145-147.

72. Moorcroft, M.J., et al., *In situ oligonucleotide synthesis on poly(dimethylsiloxane): a flexible substrate for microarray fabrication.* Nucleic Acids Research, 2005. **33**(8).

73. Kanai, M., et al., *PDMS microfluidic devices with PTFE passivated channels.* Proceedings Of The 7th International Conference on Miniaturized Chemical and Biochemical Analysis Systems, 2003: p. 429-432.

74. Chaudhury, M.K. and G.M. Whitesides, *Direct Measurement Of Interfacial Interactions Between Semispherical Lenses And Flat Sheets Of Poly(Dimethylsiloxane) And Their Chemical Derivatives.* Langmuir, 1991. **7**(5): p. 1013-1025.

75. Watson, J.M. and P.A. Payne, *A Study Of Organic-Compound Pervaporation Through Silicone-Rubber.* Journal Of Membrane Science, 1990. **49**(2): p. 171-205.

76. He, M.Y., C.H. Sun, and D.T. Chiu, *Concentrating solutes and nanoparticles within individual aqueous microdroplets.* Analytical Chemistry, 2004. **76**(5): p. 1222-1227.

77. Spring, K.R. and M.W. Davidson, *Properties of Microscope Objectives.* http://www.microscopyu.com/articles/optics/objectiveproperties.html.

78. Zaslavsky, B.Y., et al., *Phase-Separation In Aqueous Poly(Ethylene Glycol)-(Nh4)2so4 Systems And Some Physicochemical Properties Of The Phases.* Journal Of Colloid And Interface Science, 1990. **137**(1): p. 147-156.

79. Debendetti, P.G., *Metastable Liquids: Concepts and Principles*. 1996: Princeton University Press.

80. Berland, C.R., et al., *Solid Liquid-Phase Boundaries Of Lens Protein Solutions.* Proceedings Of The National Academy Of Sciences Of The United States Of America, 1992. **89**(4): p. 1214-1218.

81. Garcia-Ruiz, J.M., *Nucleation of protein crystals.* Journal Of Structural Biology, 2003. **142**(1): p. 22-31.

82. Chayen, N.E., *Methods for separating nucleation and growth in protein crystallisation.* Progress In Biophysics & Molecular Biology, 2005. **88**(3): p. 329-337.

83. Chayen, N.E., *Turning protein crystallisation from an art into a science.* Current Opinion In Structural Biology, 2004. **14**(5): p. 577-583.

84. Hansen, C.L., M.O.A. Sommer, and S.R. Quake, *Systematic investigation of protein phase behavior with a microfluidic formulator*. Proceedings of the National Academy of Sciences of the United States of America, 2004. **101**(40): p. 14431-14436.

85. Torronen, A., A. Harkki, and J. Rouvinen, *3-Dimensional Structure Of Endo-1,4-Beta-Xylanase-Ii From Trichoderma-Reesei - 2 Conformational States In The Active-Site*. Embo Journal, 1994. **13**(11): p. 2493-2501.

86. Dashek, W., *Methods in Plants Biochemistry and Molecular Biology*. 1997: CRC Press. 457.

87. Muschol, M. and F. Rosenberger, *Liquid-liquid phase separation in supersaturated lysozyme solutions and associated precipitate formation/crystallization.* Journal of Chemical Physics, 1997. **107**(6): p. 1953-1962.

88. Alderton, G., W.H. Ward, and H.L. Fevold, *Isolation Of Lysozyme From Egg White*. Journal Of Biological Chemistry, 1945. **157**(1): p. 43-58.